PIE ON SAFETY-TESTED AGR-1 COMPACTS 4-1-2 AND 4-4-3

April 2014

J.D. Hunn, R.N. Morris, C.A. Baldwin, F.C. Montgomery, and T.J. Gerczak

Introduction

Post-irradiation examination (PIE) is being performed in support of tristructural isotropic (TRISO) coated particle fuel development and qualification for High Temperature Gas-cooled Reactors (HTGRs). AGR-1 was the first in a series of TRISO fuel irradiation experiments initiated in 2006 under the Advanced Gas Reactor (AGR) Fuel Development and Qualification Program; this work continues under the current Department of Energy Office of Nuclear Energy's Next Generation Nuclear Plant (NGNP) initiative. AGR-1 fuel compacts were fabricated at Oak Ridge National Laboratory (ORNL) in 2006 and irradiated for 3 years in the Advanced Test Reactor (ATR) at Idaho National Laboratory (INL) to demonstrate and evaluate fuel performance under HTGR irradiation conditions. PIE is being performed at INL and ORNL to study how the fuel behaved during irradiation, and to test fuel performance during exposure to elevated temperatures at or above temperatures that could occur during a depressurized conduction cooldown event. In FY2011 through mid FY2014, ORNL completed the scheduled PIE on ten compacts from the AGR-1 irradiation test. This PIE included three compacts (Compacts 6-1-1, 4-4-2, and 5-2-3) examined in the as-irradiated condition [Hunn et al. 2012-3], six compacts (Compacts 6-4-3, 3-3-2, 3-2-2, 6-2-1, 3-3-1, and 4-4-1) subjected to safety testing at 1600–1800°C and post-safety testing examination similar to the PIE performed on the as-irradiated compacts [Hunn et al. 2012-3; Hunn et al. 2012-4; Hunn 2013-3], and one compact (Compact 6-4-2) that was sectioned and polished for materialographic inspection [Hunn, Savage, and Kehn 2012]. This report summarizes recent PIE completed at ORNL in FY2014 on two additional compacts: Compact 4-1-2 (AGR-1 Variant 3 fuel safety tested at 1600°C) and Compact 4-4-3 (AGR-1 Variant 3 fuel safety tested at 1700°C).

AGR-1 Compact 4-1-2 was irradiated to an average calculated burnup of 17.39% fissions per initial metal atom (FIMA) and an average calculated fast fluence of $3.72 \cdot 10^{25}$ n/m^2 [Sterbentz 2013], at a calculated volume-averaged and time-averaged temperature of approximately 1042°C [Hawkes 2012]. AGR-1 Compact 4-4-3 was irradiated to an average calculated burnup of 18.99% FIMA and an average calculated fast fluence of $4.06 \cdot 10^{25}$ n/m^2 [Sterbentz 2013], at a calculated volume-averaged and time-averaged temperature of approximately 1059°C [Hawkes 2012]. The two compacts were subjected to

safety testing in the ORNL Core Conduction Cooldown Test Facility (CCCTF). After completion of the safety testing, the compacts were examined with a standard set of analyses that included the following: (1) detection of exposed fission products and actinides by Deconsolidation-Leach-Burn-Leach (DLBL), (2) measurement of gamma-emitting isotopic inventory within individual particles with the Irradiated Microsphere Gamma Analyzer (IMGA), and (3) microstructural examination by x-ray tomography and materialography. The equipment and methods used for safety testing and post-safety testing PIE are summarized in the next section of this report, and have previously been described in detail [Baldwin et al. 2012, Hunn et al. 2013-1]. This report also provides a brief summary of the results of the safety testing and subsequent PIE. Preliminary trends are discussed, but final conclusions will require the support of additional data and further analysis of other compacts. Reports are being generated for each AGR-1 compact after PIE is complete that describe in detail the examinations performed and fully document the data obtained, and a final AGR-1 PIE summary report will compile all available data and provide a more comprehensive analysis of the AGR-1 fuel performance.

Standard examination procedure [extracted from Hunn et al. 2013-3]

Safety testing was performed in flowing helium, with compacts held at the maximum test temperature for 300 hours. During the test period, metallic elements released from the compacts were collected by a water-cooled cold finger at the top of the CCCTF furnace, and gaseous fission products were extracted from the helium sweep gas as it passed through liquid nitrogen-cooled cold traps located downstream. Deposition cups attached to the in-furnace cold finger were periodically removed and analyzed by gamma spectrometry and the sweep gas traps were constantly monitored for gamma activity throughout each run.

After completion of the safety testing, acid leaching and additional analyses were performed on the deposition cups and CCCTF furnace internals (graphite fuel holder, tantalum furnace liner, and tantalum gas inlet line). The average deposition cup collection efficiency for each detected isotope was determined as the ratio of the cumulative amount on all the deposition cups to the total detected on the cups and other CCCTF internal components. The measured data for each individual deposition cup were adjusted by these collection efficiencies to estimate the time-dependent release of each detected isotope from the compact throughout the safety test.

Additional post-safety test PIE was also performed on each compact (leach-burn-leach, individual particle gamma spectrometry, x-ray tomography, and materialography). Compacts were first electrolytically deconsolidated in nitric acid to break up the matrix carbon and release the TRISO-coated particles from the compact. Particles and matrix residue were then leached twice with hot nitric acid in a Soxhlet extractor to dissolve any soluble elements in the matrix residue or on the surface of the particles. This leaching step will also dissolve uranium in exposed kernels from particles with fractured TRISO coatings.

After the deconsolidation-leach (DL), if significant cesium release was detected during the safety test, then TRISO-coated particles were separated out from the matrix residue for IMGA survey (this was the case for Compact 4-1-2). Particles were separated from the matrix residue by first boiling in nitric acid to clean off any residual matrix from the outer surface of the TRISO particles, and then washing the matrix residue and acid through a sieve with 500-μm-square holes. The washed and dried particles were then transferred to the IMGA hot cell for gamma analysis. The matrix residue was dried and burned at 750°C to oxidize any remaining elements. Boiling nitric acid was then used to leach the ash. After IMGA examination, approximately 90% of the particles were returned to the Soxhlet thimble for burn-leach (BL). During this BL, the outer pyrocarbon and elements remaining on the surface of the particles that were not dissolved during the pre-burn leach are oxidized. The burn-leach will also detect exposed uranium in any particles with through-wall defects in the SiC that were protected by intact pyrocarbon during the pre-burn leaching and not removed due to low cesium content by IMGA. If cesium release was not detected during the safety test (as was the case for Compact 4-4-3), then particles and matrix were burned and leached together. The flow chart in Figure 1 outlines the DLBL process.

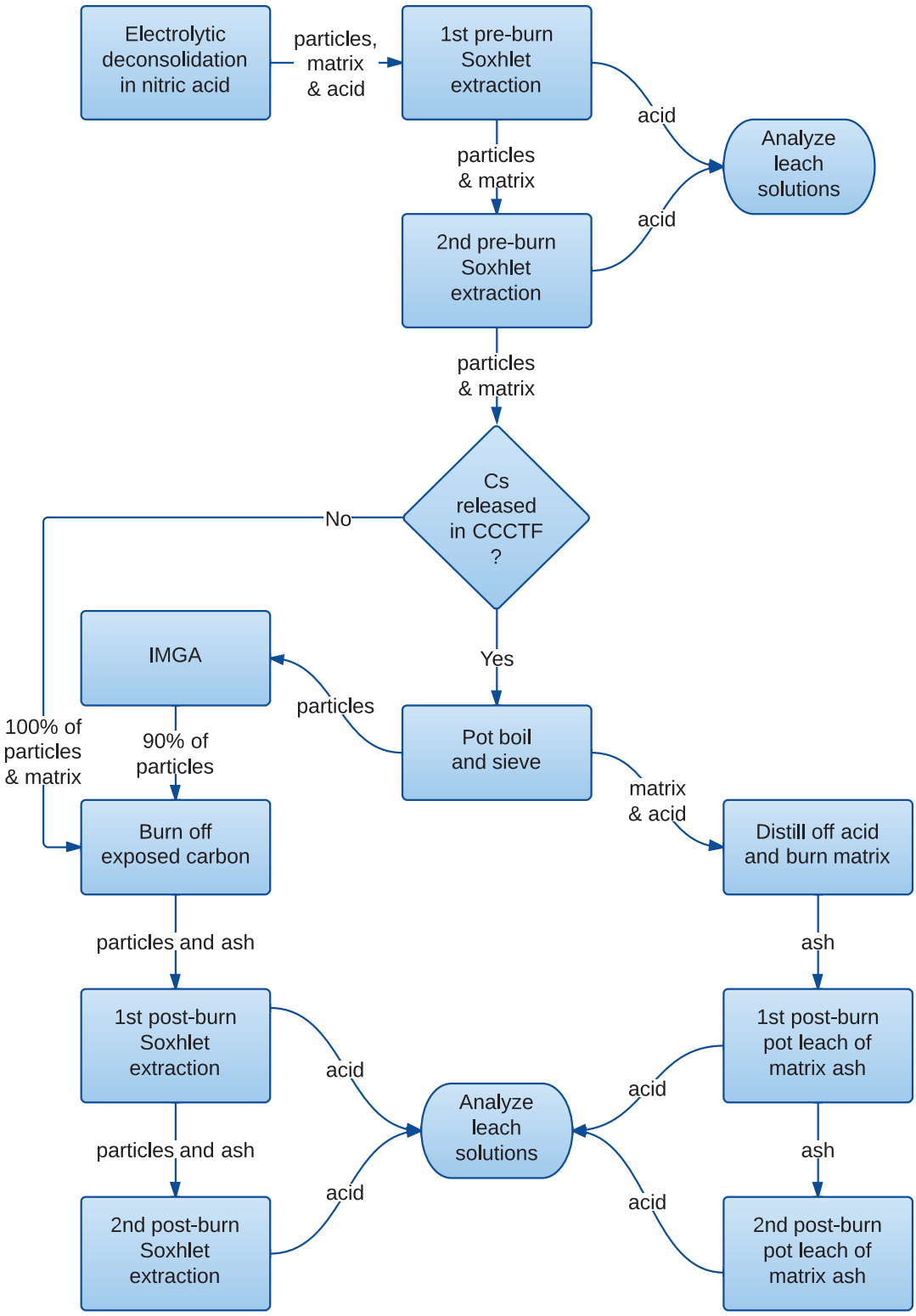

Figure 1. Flow chart of the DLBL process.

TRISO-coated particles from compacts that released significant cesium were surveyed for ^{137}Cs and ^{144}Ce inventory with the IMGA using a 50 sec counting time. The IMGA uses a computer-controlled pneumatic particle manipulator to remove individual particles from a hopper, transfer them to a gamma scanning station, and then sort them into specified containers based on the measured gamma spectra. This process requires about two weeks to analyze and sort all 4100+ particles from each compact. Particles were primarily sorted according to their ^{144}Ce content, where particles with significantly low ^{144}Ce inventory were placed in a separate receptacle for further analysis. Particles with essentially normal ^{144}Ce inventory were sorted by their $^{137}Cs/^{144}Ce$ ratio, and particles with a low ratio were deposited into designated vials. Particles with significantly below average cerium content could contain abnormally small kernels or kernels that were leached by the DL process. A low $^{137}Cs/^{144}Ce$ ratio implies particles have preferentially lost cesium, which generally indicates a through-wall defect in the SiC layer. After the IMGA survey, particles identified as having anomalous^{144}Ce or ^{137}Cs inventory were surveyed for 5 hours to increase the accuracy of the gamma spectra and measure other lower activity gamma emitters. For all compacts, about 50 randomly-selected particles were also scanned for 5 hours to examine the average inventory of various detectable isotopes, including ^{95}Zr, ^{106}Ru, ^{110m}Ag, ^{125}Sb, ^{134}Cs, ^{137}Cs, ^{144}Ce, and ^{154}Eu.

After IMGA examination, particles were selected for microstructural analysis. Particles with anomalous isotopic inventories were compared to average particles. Emphasis was given to particles that exhibited different silver retention to look for any unique features. Microstructural analysis included x-ray imaging and materialographic inspection by mechanical polishing followed by analysis using optical and scanning electron microscopes.

Three-dimensional microstructural analysis was achieved using a high-resolution x-ray tomography system specifically designed for imaging TRISO-coated particles. This system can image coating structure with resolution close to 1 μm, and has been used during AGR-1 fuel development to characterize and understand defect structures in unirradiated, as-fabricated particles in a manner not previously available. For AGR-1 PIE, a shielded container has been designed for mounting irradiated particles on the x-ray tomography stage. This shielded container allows single particles to be removed from the hot cell and transported to the tomography instrument for imaging. The shielding also reduces gamma radiation interference in the detector and electronics. Radiographic image sets using 3200 particle orientations were acquired to support high-resolution three-dimensional (3D) tomographic reconstruction of the irradiated particle microstructure.

Mechanical polishing to reveal particle cross sections was achieved by mounting particles in epoxy and grinding/polishing with a Buehler Minimet 1000. Vacuum back-potting was used to prevent damage to the internal structure and improve the quality of the final polished cross section. Kernels and coating layers were imaged using an optical microscope. Scanning electron microscopy (SEM) was performed on some samples to provide additional information. Secondary-electron image (SEI) and backscattered-electron composition (BEC) modes were used to examine the structure and detect heavy metal clusters outside of the kernel, which were identified with Energy Dispersive Spectrometry (EDS).

Safety testing results

Compact 4-1-2 (AGR-1 Variant 3 fuel safety tested at 1600°C) and Compact 4-4-3 (AGR-1 Variant 3 fuel safety tested at 1700°C) were each held at the maximum test temperature for 300 hours in flowing helium using the ORNL CCCTF. The purpose of these tests was to evaluate the effect of elevated temperature on the fuel microstructure and radioisotope retention. The results of the two safety tests have been previously reported [Hunn et al. 2013-2] and are briefly discussed in this section. Overall, the coated particle fuel appears to have continued to retain radioisotopes generated by the three-year irradiation test. No significant ^{85}Kr was detected in the helium sweep gas throughout both safety tests. This indicates that every particle had at least one intact gas-retentive layer: inner pyrocarbon (IPyC), silicon carbide (SiC), or outer pyrocarbon (OPyC). However, some radioisotopes came out of the compacts and were detected on the deposition cups and furnace internals (Table 1).

Table 1. Cumulative releases of radioactive isotopes at the end of safety testing

Isotope	Compact 4-1-2 (1600°C)	Compact 4-4-3 (1700°C)
^{85}Kr	<1E-6 (<0.004)	<1E-6 (<0.004)
^{90}Sr	1.43E-4 (0.59)	9.67E-4 (3.99)
^{110m}Ag	5.80E-2 (239)	1.66E-1 (683)
^{134}Cs	1.66E-4 (0.69)	<1E-6 (<0.004)
^{137}Cs	1.66E-4 (0.69)	<1E-6 (<0.004)
^{154}Eu	3.39E-4 (1.40)	2.90E-3 (12.0)
^{155}Eu	3.79E-4 (1.56)	2.85E-3 (11.8)

Release values are reported as a fraction of the calculated post-irradiation compact inventory [from Sterbentz 2013], with the equivalent number of exposed kernels shown in parentheses, which was calculated as the compact inventory fraction times the average number of particles in a Capsule 4 compact (4126 particles/compact).

Cesium release during safety testing higher than a compact fraction of ~1E-5 is a good indicator for the presence of particles with breached SiC. The cesium release from Compact 4-4-3 was too low to measure above the background that can come from other radioactive contamination in the hot cell environment, indicating that all SiC layers remained intact. In contrast, Compact 4-1-2 showed a total cesium release of ~69% of the average inventory in a single irradiated 4-1-2 particle; this is equivalent to the amount of cesium that would be expected to escape from 1–2 particles with breached SiC. Figure 2 shows the safety test temperature profile and the estimated time-dependent radioisotope releases for Compact 4-1-2. The plotted fractional release values are the cumulative amount of each radioisotope collected on the deposition cups, adjusted for radioactive decay and average collection efficiency, and divided by the predicted compact inventory for that isotope at the end of the irradiation [from Sterbentz 2013]. Most of the released cesium was collected during the first 14 hours at 1600°C, indicating that the SiC was breached during this period. There was a slightly elevated quantity of cesium (6E-6) on the first cup exchanged one hour after reaching 1600°C, which could have come from the failing SiC or from contamination in the furnace, but if a SiC layer had failed during ramp up, more cesium would be expected after 1 hour at 1600°C.

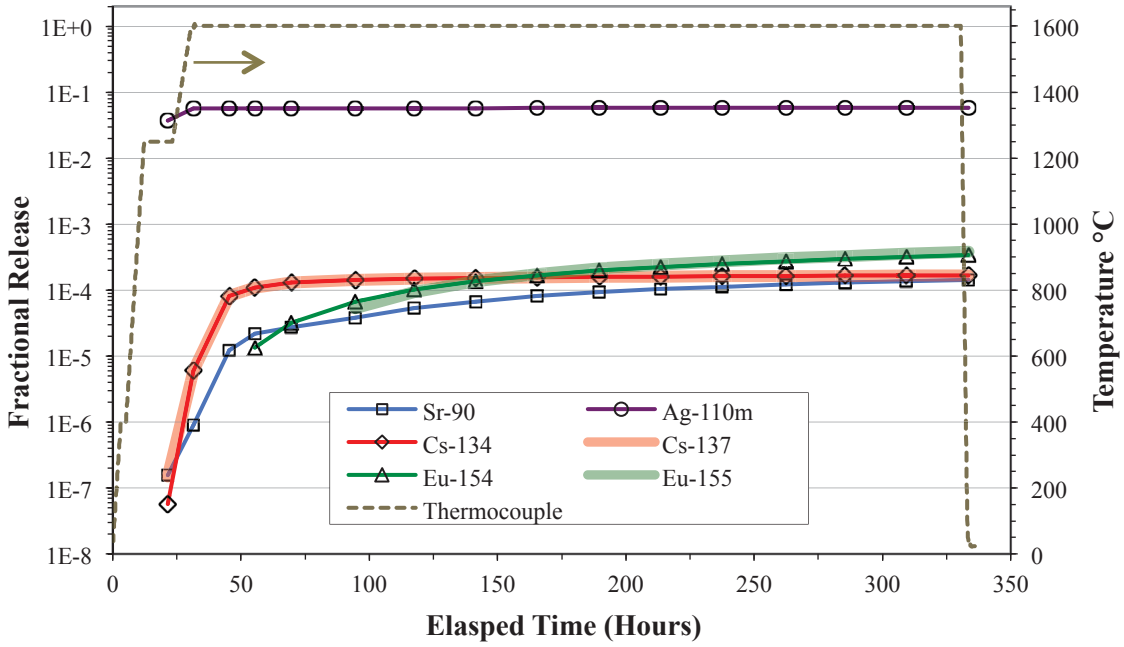

Figure 2. Release of radioactive isotopes from Compact 4-1-2 during safety testing to 1600°C.

As a fraction of the total compact inventory, ^{110m}Ag release was significantly higher than any other detected isotope (Table 1), which is the typical behavior observed in all AGR-1 safety tests. Given that most of the silver release during safety testing is detected on the cups removed soon after ramping up the temperature, and many particles still retain a large fraction of their silver inventory inside of the SiC layer at the end of each safety test, it is hypothesized that most of the silver released during safety testing is coming from locations already outside of intact SiC, having been previously transported through intact SiC during the irradiation period. The higher silver release from Compact 4-4-3 is not necessarily related to the higher safety test temperature, where both safety test temperatures are expected to result in release of close to 100% of the silver not retained by intact SiC; it is possible that Compact 4-4-3 simply had more silver retained in the OPyC and matrix graphite at the end of irradiation. However, thermal cycling may have been a contributing factor to the higher silver release during the Compact 4-4-3 safety test. Figure 3 shows the time-dependent data for this safety test. An interruption at the start of the test due to insufficient cooling water is reflected in the drop from 1700°C back to room temperature that occurred 33 hours into the test. Table 2 summarizes the fraction of released ^{110m}Ag on each deposition cup; additional ^{110m}Ag was released after the thermal cycling of the compact from 1700–20–1700°C. A similar effect was observed during safety testing of Compacts 3-2-2 and 3-3-2 and was intentionally investigated at the conclusion on the Compact 3-3-2 safety test [Hunn et al. 2012-2], where additional ^{110m}Ag was released by thermal cycling to 1600°C, even after negligible release was observed for 270 h at 1600°C.

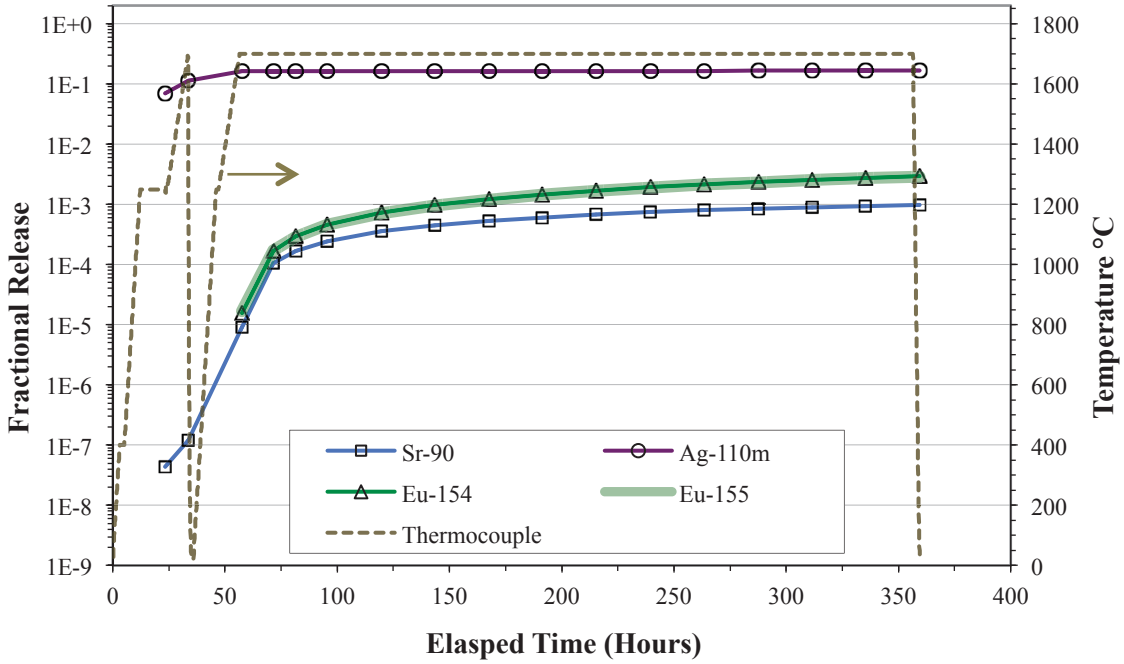

Figure 3. Release of radioactive isotopes from Compact 4-4-3 during safety testing to 1700°C.

Table 2. Fraction of released ^{110m}Ag collected by each cup

Cup	Compact 4-1-2 (1600°C)	Compact 4-4-3 (1700°C)
1	63.7% (12 h, 20–1250°C + 9 h, 1250°C)	42.1% (12 h, 20–1250°C + 11 h at 1250°C)
2	33.1% (9 h, 1250–1600°C + 1 h at 1600°C)	25.2% (10 h, 1250–1700°C + 0 h at 1700°C)
3	0.3% (14 h at 1600°C)	30.2% (23 h, 1700–20–1700°C + 1 h at 1700°C)
4	0.2% (10 h at 1600°C)	0.4% (14 h at 1700°C)
5	0.2% (14 h at 1600°C)	0.2% (10 h at 1700°C)

Europium and strontium also showed higher release during safety testing from Compact 4-4-3 than from Compact 4-1-2 (Table 1), but this may also be independent of the difference in test temperature or possible release through intact SiC. Like silver, europium and strontium safety test release can be dominated by what is already outside of intact SiC at the start of the safety test, and the measured releases from these two compacts were less than what has been observed trapped in the OPyC and matrix of as-irradiated compacts.

DLBL results

Table 3 summarizes the results of the DLBL analyses for some of the key isotopes generated by the irradiation test. These results indicate how much of each isotope, that was not contained within intact SiC, was detected in the compact before and after the burn step, where the burn step oxidizes exposed carbon and most exposed metallic elements not previously leached. Results are presented in terms of the compact inventory fraction and the equivalent number of exposed kernels (in parentheses). The compact inventory fraction was determined by dividing the measured amount of each isotope by the amount that was calculated to be in the fuel as a result of the three-year irradiation and subsequent radioactive decay, assuming no isotopic release during irradiation [Sterbentz 2013]. The equivalent number of exposed kernels was determined from the compact inventory fraction by multiplying by the average number of particles in each compact (4126 particles per average Capsule 4 compact). In Table 3, pre-burn data is presented in two parts. The first column of pre-burn data was obtained using the two standard pre-burn Soxhlet extractions (Figure 1). The second column of pre-burn data was obtained from additional analysis prior to the burn, as described in the table footnotes.

Table 3. Isotopes detected at various stages of DLBL analysis

Isotope	Possible Background (upper limit)	Compact 4-1-2 (1600°C)				Compact 4-4-3 (1700°C)		
		pre-burn	pre-burn*	matrix post-burn	particle post-burn	pre-burn	pre-burn*	post-burn
^{90}Sr	5E-7 (0.002)	1.98E-5 (0.08)	4.50E-6 (0.02)	5.21E-5 (0.21)	4.71E-5 (0.19)	1.03E-04 (0.42)	7.41E-07 (0.003)	1.78E-04 (0.74)
^{105}Pd	3E-4 (1.2)	<6.01E-6 (<0.02)	<8.24E-6 (<0.03)	2.04E-5 (0.08)	<4.43E-5 (<0.18)	<1.72E-5 (<0.07)	<1.85E-5 (<0.08)	<4.23E-5 (<0.17)
^{106}Ru	4E-7 (0.002)	<7.51E-7 (<0.003)	6.96E-6 (0.02)	4.57E-6 (0.019)	<1.28E-6 (<0.005)	<1.19E-6 (<0.005)	<4.52E-7 (<0.002)	<2.73E-6 (<0.011)
^{110m}Ag	<5E-5 (<0.2)	<8.71E-5 (<0.36)	<8.12E-5 (<0.34)	<8.96E-5 (<0.37)	<1.49E-4 (<0.62)	<1.28E-4 (<0.53)	<5.08E-5 (<0.21)	<2.98E-4 (<1.23)
^{125}Sb	1E-6 (0.004)	<2.46E-6 (<0.010)	2.24E-5 (0.09)	7.53E-6 (0.03)	<4.03E-6 (<0.016)	<3.30E-6 (0.014)	<1.32E-6 (0.006)	<6.55E-6 (0.03)
^{134}Cs	2E-7 (0.0008)	1.25E-7 (0.0005)	1.20E-6 (0.005)	2.95E-6 (0.012)	3.55E-7 (0.0015)	2.94E-7 (0.0012)	2.09E-8 (0.0001)	1.70E-6 (0.007)
^{137}Cs	6E-7 (0.002)	3.94E-7 (0.002)	1.74E-6 (0.007)	4.85E-6 (0.02)	5.76E-6 (0.02)	2.79E-6 (0.012)	6.35E-7 (0.003)	2.80E-6 (0.012)
^{144}Ce	5E-7 (0.002)	1.28E-5 (0.05)	1.47E-4 (0.61)	5.26E-5 (0.22)	4.75E-7 (0.002)	1.08E-5 (0.04)	1.65E-7 (0.0007)	5.45E-5 (0.22)
^{154}Eu	3E-6 (0.01)	5.02E-5 (0.21)	1.10E-5 (0.05)	1.96E-4 (0.81)	1.41E-4 (0.58)	2.29E-4 (0.95)	2.58E-6 (0.011)	9.21E-4 (3.80)
^{155}Eu	2E-6 (0.01)	6.15E-5 (0.25)	<6.54E-6 (<0.03)	2.34E-4 (0.97)	1.57E-4 (0.65)	2.64E-4 (1.09)	3.29E-6 (0.014)	1.07E-3 (4.41)

Values are reported as the fraction of compact inventory and the equivalent number of exposed kernels (in parentheses).
"<" indicates the measured signal was below a minimum detectable limit; "n.m." indicates a value was not measured.
Compact 4-1-2 pre-burn* data are additional results from a third acid leach and water rinse prior to the burn.
Compact 4-4-3 pre-burn* data are additional results from a water rinse prior to the burn.
Numbers in gray are below estimated upper limits for possible background from hot cell contamination, determined by analysis of acid rinses as described in [Hunn et al. 2103-1].

Table 3 continued. Isotopes detected at various stages of DLBL analysis

Isotope	Possible Background (upper limit)	Compact 4-1-2 (1600°C)				Compact 4-4-3 (1700°C)		
		pre-burn	pre-burn*	matrix post-burn	particle post-burn	pre-burn	pre-burn*	post-burn
^{152}Sm	8E-6 (0.03)	8.56E-5 (0.35)	9.77E-5 (0.40)	1.92E-4 (0.79)	1.91E-4 (0.79)	1.61E-4 (0.67)	<6.68E-6 (<0.03)	4.54E-4 (1.87)
^{235}U	2E-6 (0.01)	1.35E-6 (0.006)	2.19E-4 (0.90)	5.43E-6 (0.02)	5.46E-5 (0.23)	5.48E-6 (0.02)	1.17E-6 (0.005)	5.52E-6 (0.02)
^{238}U	3E-6 (0.01)	2.22E-6 (0.009)	2.30E-4 (0.95)	9.03E-6 (0.04)	5.04E-6 (0.02)	9.11E-6 (0.04)	1.42E-6 (0.006)	6.47E-6 (0.03)
^{239}Pu	2E-6 (0.01)	1.66E-5 (0.07)	1.27E-4 (0.52)	5.23E-5 (0.22)	2.40E-5 (0.10)	1.44E-5 (0.06)	6.13E-7 (0.003)	4.39E-5 (0.18)
^{240}Pu	3E-6 (0.01)	1.80E-5 (0.07)	1.27E-4 (0.52)	5.45E-5 (0.23)	2.52E-5 (0.10)	1.64E-5 (0.07)	6.84E-7 (0.003)	4.86E-5 (0.20)

Values are reported as the fraction of compact inventory and the equivalent number of exposed kernels (in parentheses).
Compact 4-1-2 pre-burn* data are additional results from a third acid leach and water rinse prior to the burn.
Compact 4-4-3 pre-burn* data are additional results from a water rinse prior to the burn.
Numbers in gray are below estimated upper limits for possible background from hot cell contamination, determined by analysis of acid rinses as described in [Hunn et al. 2103-1].

Detection of uranium during DLBL is a good indicator for exposed kernels. If none of the TRISO layers are intact, then acid will dissolve uranium in the kernel during the first pre-burn leach. If good pyrocarbon protects a SiC that is not intact, then the burn step will remove the pyrocarbon and expose the kernel to post-burn leaching. Greater than 90% of the uranium in an exposed kernel is typically leached by the hot acid. Compact 4-4-3 DLBL showed no indication of exposed kernels in pre-burn or post-burn leaching; this was in good agreement with the results of the safety test, where krypton and cesium releases were negligible.

Based on the measured cesium detected on the deposition cups and the absence of ^{85}Kr in the sweep gas, Compact 4-1-2 was expected to contain 1–2 particles with breached SiC but at least one intact pyrocarbon layer. DLBL of this compact showed no exposed kernels in the initial pre-burn leaching, verifying the expectation from the lack of ^{85}Kr release during safety testing. However, during a third pre-burn leach, uranium was detected equivalent to one kernel's inventory. Subsequent analysis (discussed below) showed that this uranium came from one particle with breached SiC whose kernel was exposed during the third Soxhlet extraction through loss of the OPyC layer. Exposure of this kernel during the third pre-burn leach also resulted in an increased concentration in the leachant of the other measured isotopes (especially ^{144}Ce, ^{152}Sm, ^{239}Pu, and ^{240}Pu). Only small amounts of cesium and europium were detected in the third pre-burn leach when the kernel was exposed, presumably because they had already been released during safety testing (IMGA data discussed below showed very low amounts remaining in the particle).

DLBL of as-irradiated compacts typically detects a higher inventory fraction of exposed silver than any other element. Table 3 shows that no exposed ^{110m}Ag could be detected in the compacts after safety testing; this confirms that silver outside of intact SiC is readily diffusing out of the compacts at 1600°C. The amount of exposed ^{105}Pd remaining in the compacts after safety testing was also unusually low compared to what has been observed in as-irradiated compacts; more recent safety tests include analysis for palladium on the furnace components to quantify its release.

The amount of ^{90}Sr and ^{154}Eu detected by DLBL to be outside of intact SiC in Compact 4-4-3 was 23% and 28% of the amounts released from the compact during the safety test at 1700°C, respectively. Europium and strontium appear to move slowly through the carbonaceous OPyC, compact matrix, and CCCTF graphite holder during safety testing. Compact 4-1-2 also retained about 25% of its exposed europium and strontium.

IMGA results

An IMGA survey of all available particles deconsolidated from Compact 4-1-2 was performed using a 50-second counting time. Figure 4 is a histogram of the collected data for ^{137}Cs content, plotted as the ratio of the measured versus calculated inventory and adjusted for particle-to-particle variation in fissionable material and burn-up using the measured ^{144}Ce activity, as described in [Hunn et al. 2013-1]. The overall distribution indicates that the typical particle retained ^{137}Cs well, and the calculated inventory appears to be accurate to within a few percent. However, one particle with abnormally low ^{137}Cs retention (relative to ^{144}Ce) can be seen to the left of the main distribution; this particle (412-SP05) was automatically sorted out during the IMGA survey for further analysis.

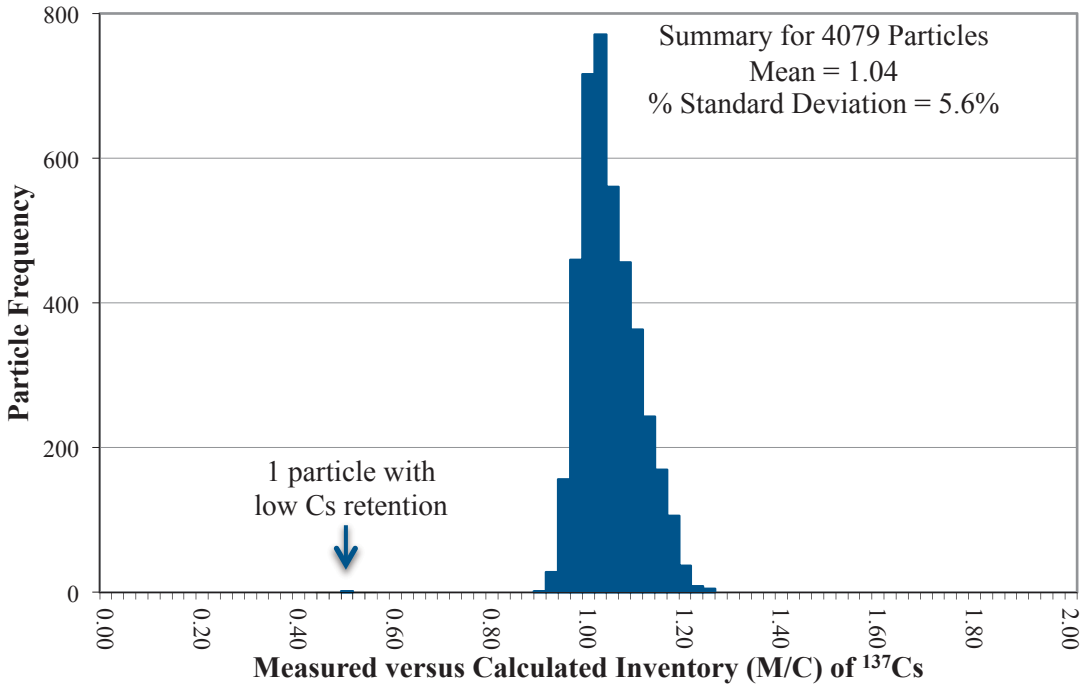

Figure 4. Estimated fraction of ^{137}Cs retained in particles from Compact 4-1-2, based on calculated inventory and adjusted for variation in fissionable material and burn-up using the measured ^{144}Ce activity.

The particle with relatively low ^{137}Cs retention (Particle 412-SP05), along with four particles equally low in both ^{137}Cs and ^{144}Ce and 50 randomly-selected particles were loaded into individual vials and subjected to 5-hour gamma scanning. This longer scan time provided better quantitative analysis of the cesium and cerium content, and also allowed for analysis of other lower activity gamma-emitting isotopes, such as silver and europium. By handling particles in separate vials, the individual identity of each particle was maintained through the remainder of the PIE.

Table 4 shows the measured activities for select gamma-emitting isotopes retained in Particle 412-SP05, as well as the average measured activities of the 50 randomly-selected particles and the calculated inventories of an average particle from Compact 4-1-2. The randomly-selected particles showed typical inventories for all the measured isotopes, with average activities close to the calculated values, except for ^{125}Sb and ^{154}Eu, where the calculated values have been shown to have a similar positive bias [Harp 2013]. The low cesium particle showed a below average inventory for all the measured isotopes. This was in contrast to particles with breached SiC that have released cesium in other safety tests, which typically exhibit good retention of ^{106}Ru, ^{125}Sb, and ^{144}Ce, varied retention of cesium and europium, and very low retention of ^{110m}Ag [Hunn et al. 2013-3]. The fact that Particle 412-SP05 had a below average inventory of ^{106}Ru, ^{125}Sb, and ^{144}Ce provides further evidence that the kernel was exposed during pre-burn leaching.

Table 4: Radioactive isotopes detected in particles from Compact 4-1-2.

	Activity of select gamma-emitting isotopes in Bq/particle						
	^{106}Ru	^{110m}Ag	^{125}Sb	^{134}Cs	^{137}Cs	^{144}Ce	^{154}Eu
Calculated inventory for an average particle from 4-1-2	1.39E7	5.29E4	3.23E5	5.31E6	4.27E6	5.30E7	1.78E5
Average measured inventory of 50 random particles	1.42E7 (1.02)	4.65E4 (0.88)	2.26E5 (0.70)	5.45E6 (1.03)	4.38E6 (1.03)	5.43E7 (1.02)	1.57E5 (0.88)
Percent standard deviation in average measured inventory	9.37	23.26	7.93	10.39	7.31	7.43	9.55
Low-cesium particle (412-SP05)	1.16E7 (0.83)	<5.5E3 (<0.10)	9.53E4 (0.30)	3.53E4 (0.01)	6.70E4 (0.02)	1.78E6 (0.03)	1.50E3 (0.01)

All activities are decay-corrected to one day after end of irradiation (11/07/2009 at 1200 GMT).
Values in parentheses are the ratios of the average measured inventories to the average calculated inventories, but do not include the adjustment for variation in fissile material or burnup used in IMGA histograms.

The four particles identified by the 50-second scan IMGA survey to be equally low in both ^{137}Cs and ^{144}Ce all contained about 25% of the cesium and cerium found in an average particle from Compact 4-1-2, but were relatively high in ^{106}Ru, ^{110m}Ag, ^{125}Sb, and ^{154}Eu. Similar particles have been found in other compacts and analysis is consistent with the assumption that these particles had abnormally low as-fabricated ^{235}U enrichment [Hunn et al. 2013-1, page 36].

The 50 randomly-selected Compact 4-1-2 particles exhibited a relatively broad distribution in the retained ^{110m}Ag inventory (Figure 5), with about 80% of the particles centered around a measured to calculated ratio of one and about 20% making up a low-end tail. The Compact 4-1-2 ^{110m}Ag distribution was similar to the observed ^{110m}Ag inventory distribution in as-irradiated Compact 4-4-2 [Hunn et al. 2013-1], and may not be different from what would have been measured prior to safety testing.

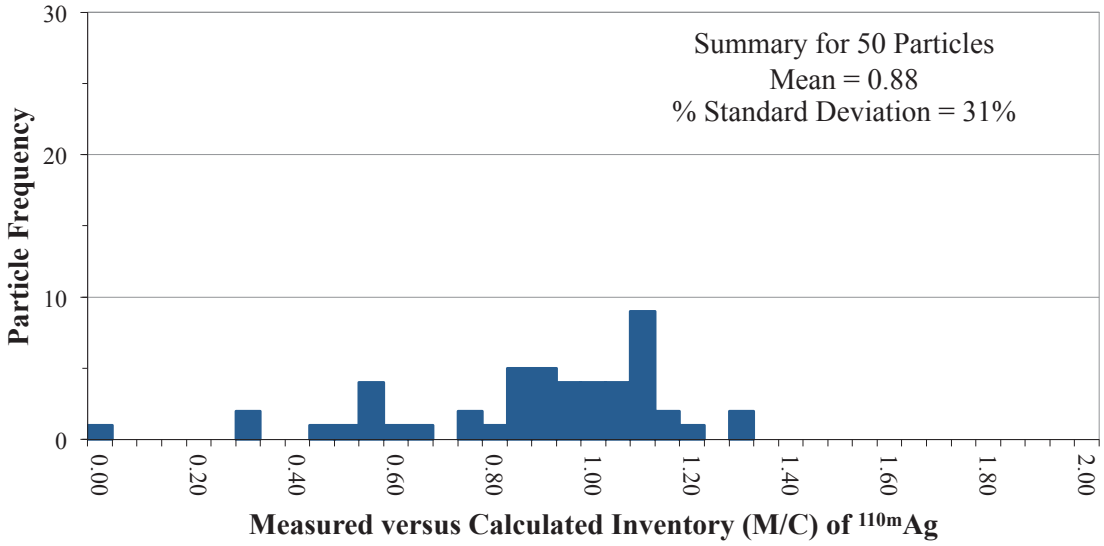

Figure 5. Ratio of ^{110m}Ag retained in 50 particles randomly-selected from Compact 4-1-2 versus the calculated inventory, and adjusted for variation in fissile material and burnup using the ^{137}Cs activity. Note that the ^{110m}Ag activity in these particles was very low at the time of analysis and uncertainty in peak analysis ranged from ~11% at the upper end of the distribution to ~30% at the lower end. The one particle with zero measurable inventory probably contained less than a minimum detectable activity of ~27%.

IMGA survey of all the particles from Compact 4-4-3 was not performed because there was no indication during safety testing for the presence of particles with breached SiC. Results of 5-hour gamma scanning of 43 randomly-selected particles from Compact 4-4-3 (Table 5) were similar in most ways to the results for the 50 randomly-selected particles from Compact 4-1-2 (Table 4), with silver retention being a notable difference, where the ratio of the average ^{110m}Ag activity versus the calculated inventory was measurably lower for the Compact 4-4-3 random sample. Figure 6 shows a broad range of ^{110m}Ag retention in the Compact 4-4-3 particles that was comparable to the distribution exhibited by Compact 4-4-1 particles after 1800°C safety testing [Hunn et al. 2013-3]. (Compact 4-4-1 was adjacent to Compact 4-4-3 in the AGR-1 irradiation capsule and experienced similar irradiation conditions [Collin 2012].) The lower average ^{110m}Ag inventory observed in particles recovered from Compacts 4-4-3 and 4-4-1 is consistent with the possibility of additional silver release through intact SiC during safety testing that was suggested by the secondary ^{110m}Ag releases observed after initial heat up to maximum test temperature. However, the broad variation in ^{110m}Ag retention observed in the AGR-1 test fuel requires more study before any conclusions can be drawn about such post-irradiation silver release from particles with intact SiC, and it is also possible that these two compacts experienced above average silver release during irradiation.

Table 5: Radioactive isotopes detected in particles from Compact 4-4-3.

	Activity of select gamma-emitting isotopes in Bq/particle						
	^{106}Ru	**^{110m}Ag**	**^{125}Sb**	**^{134}Cs**	**^{137}Cs**	**^{144}Ce**	**^{154}Eu**
Calculated inventory for an average particle from 4-4-3	1.55E7	6.75E4	3.49E5	6.44E6	4.68E6	5.27E7	2.00E5
Average measured inventory of 43 random particles	1.53E7 (0.99)	5.02E4 (0.74)	2.36E5 (0.68)	6.61E6 (1.03)	4.76E6 (1.02)	5.32E7 (1.01)	1.69E5 (0.84)
Percent standard deviation in average measured inventory	8.5	42	8.1	9.0	7.4	7.8	8.9

All activities are decay-corrected to one day after end of irradiation (11/07/2009 at 1200 GMT).
Values in parentheses are the ratios of the average measured inventories to the average calculated inventories, but do not include the adjustment for variation in fissile material or burnup used in IMGA histograms.

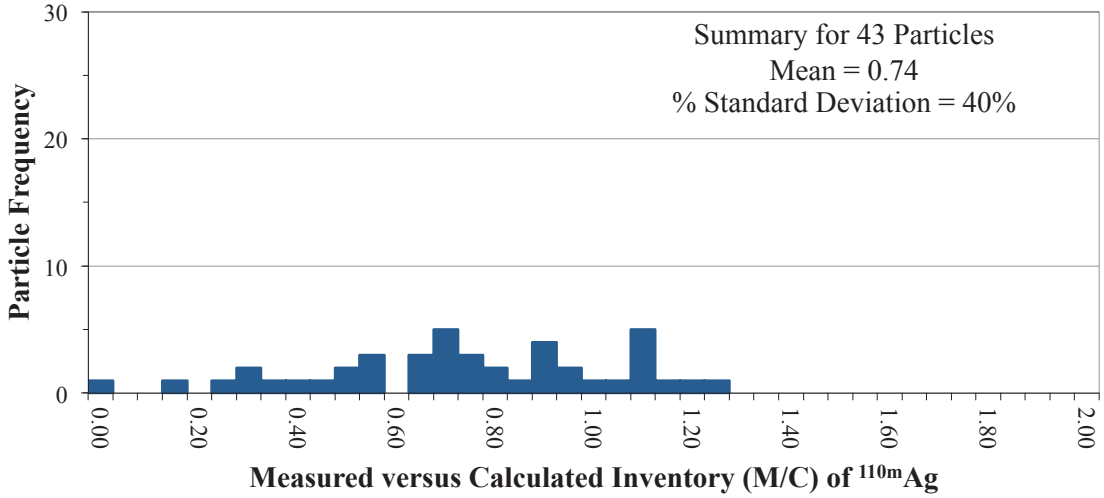

Figure 6. Ratio of ^{110m}Ag retained in 43 particles randomly-selected from Compact 4-4-3 versus the calculated inventory, and adjusted for variation in fissile material and burnup using the ^{137}Cs activity. Note that the ^{110m}Ag activity in these particles was very low at the time of analysis and uncertainty in peak analysis ranged from ~11% at the upper end of the distribution to ~30% at the lower end. The one particle with zero measurable inventory probably contained less than a minimum detectable activity of ~18%.

Microstructural analysis of individual particles

X-ray and optical microscopy on particles from randomly-selected IMGA samples

Figure 7 shows an x-ray tomograph through the midplane of a particle from Compact 4-1-2 with a measurably reduced ^{110m}Ag inventory (M/C = 0.57 from Figure 5), overlaid on a 3D visualization using the entire tomographic dataset. Three-dimensional inspection of this particle showed the common separation of buffer from IPyC due to irradiation-induced densification of the buffer. One section of the buffer was still attached to the IPyC and there were some tendrils between the buffer and IPyC where the buffer had torn away from the IPyC interface as it shrunk. No radiation-induced structural changes were observed in the three outer TRISO layers.

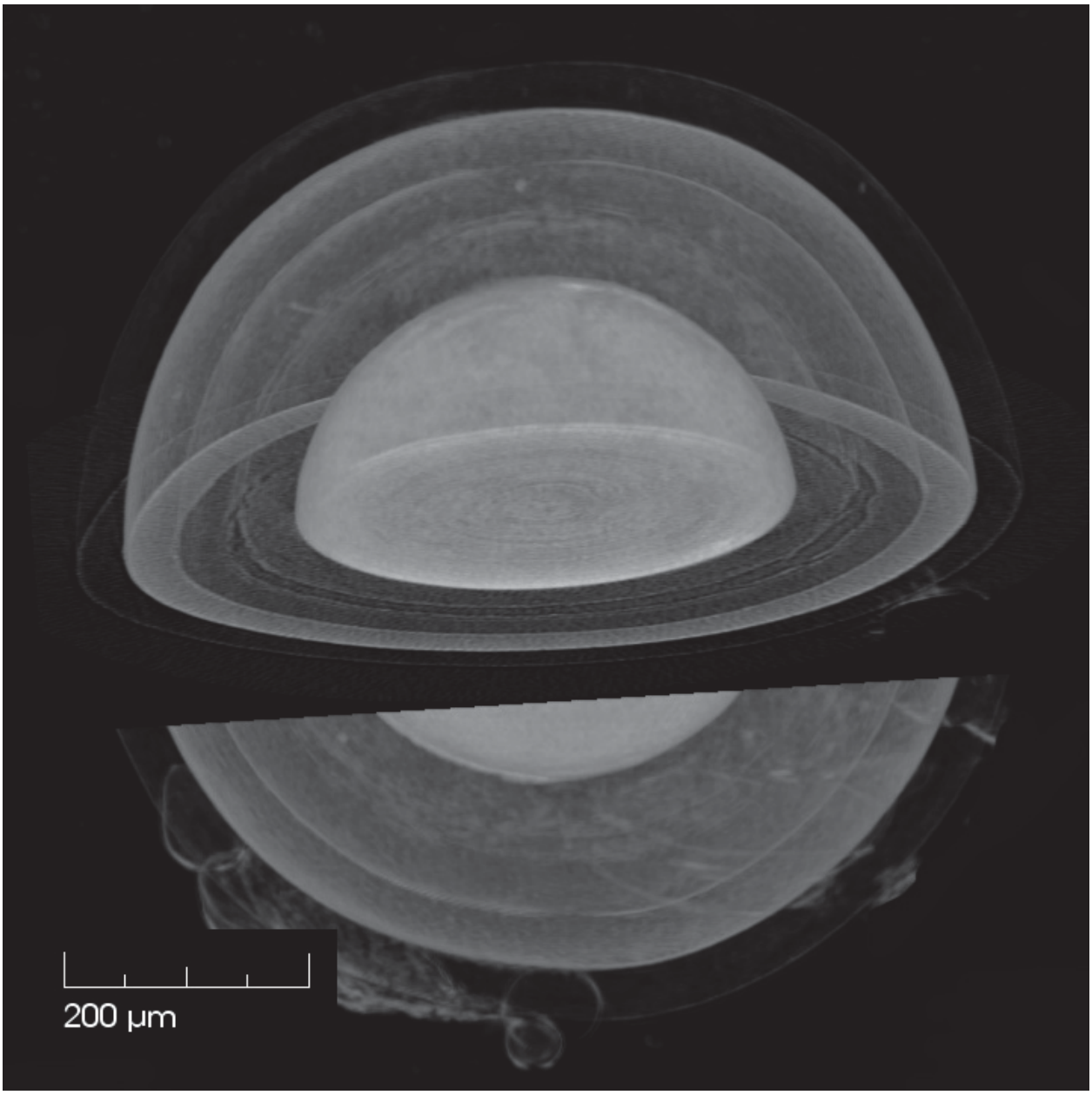

Figure 7. X-ray tomograph near midplane and 3D visualization of Particle 412-RS24 from Compact 4-1-2 with measurably reduced ^{110m}Ag inventory (M/C = 0.57). Bright features at the bottom of the particle are from bubbles in the mounting epoxy.

Two particles were selected from Compact 4-4-3 for x-ray imaging, one with below the measured average and one with above the measured average (close to the calculated average) ^{110m}Ag inventory (Figure 8). In both cases, 3D inspection of the particles showed that buffer densification had led to the buffer detaching from the IPyC without apparent damage to the IPyC or SiC (OPyC was removed during DLBL). The buffer remained attached to the IPyC at two opposing locations in both particles (only one location is visible in Figure 8b). In one case, the buffer remained intact and the kernel, which apparently increased in volume by about 60%, remained essentially spherical. In the other case, the buffer fractured and kernel material protruded into the gap between the fragments. Three-dimensional inspection of this partially-unrestrained kernel swelling showed that the kernel had protruded all the way to the IPyC layer, filling almost the entire open volume between the buffer pieces in many locations.

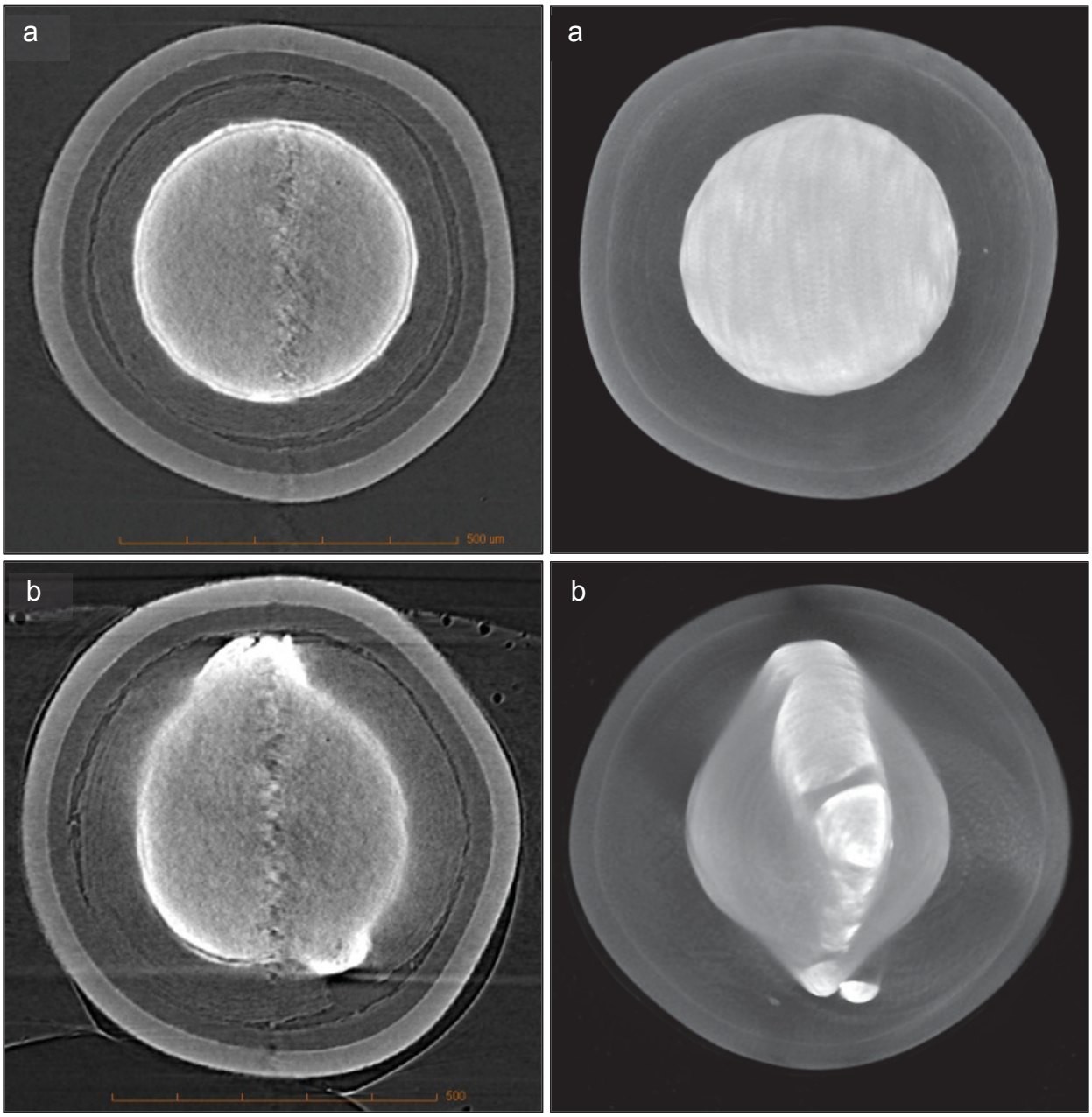

Figure 8. X-ray tomographs near midplane of particles from Compact 4-4-3 and 3D visualizations highlighting the kernel shape for a) Particle 443-RS31 with reduced ^{110m}Ag inventory (M/C = 0.36), and b) Particle 443-RS23 with close to the average calculated ^{110m}Ag inventory (M/C = 0.92).

Figure 9 shows four other particles from Compact 4-4-3 with varying ^{110m}Ag inventory, and Figure 10 shows four particles from Compact 4-1-2; these particles exhibited internal microstructures similar to the particles examined by x-ray. In this limited sampling of eleven particles from two compacts, buffer fracture with various degrees of kernel protrusion was observed in particles that had both above average and below average ^{110m}Ag inventory. Microstructural analysis of particles from other AGR-1 compacts has found similar buffer fracture in some particles with either very low or average ^{110m}Ag inventory [Hunn et al. 2013-3 and Hunn et al. 2012-3]. There does not seem to be any correlation between ^{110m}Ag inventory and the radiation-induced evolution in the buffer and kernel structures.

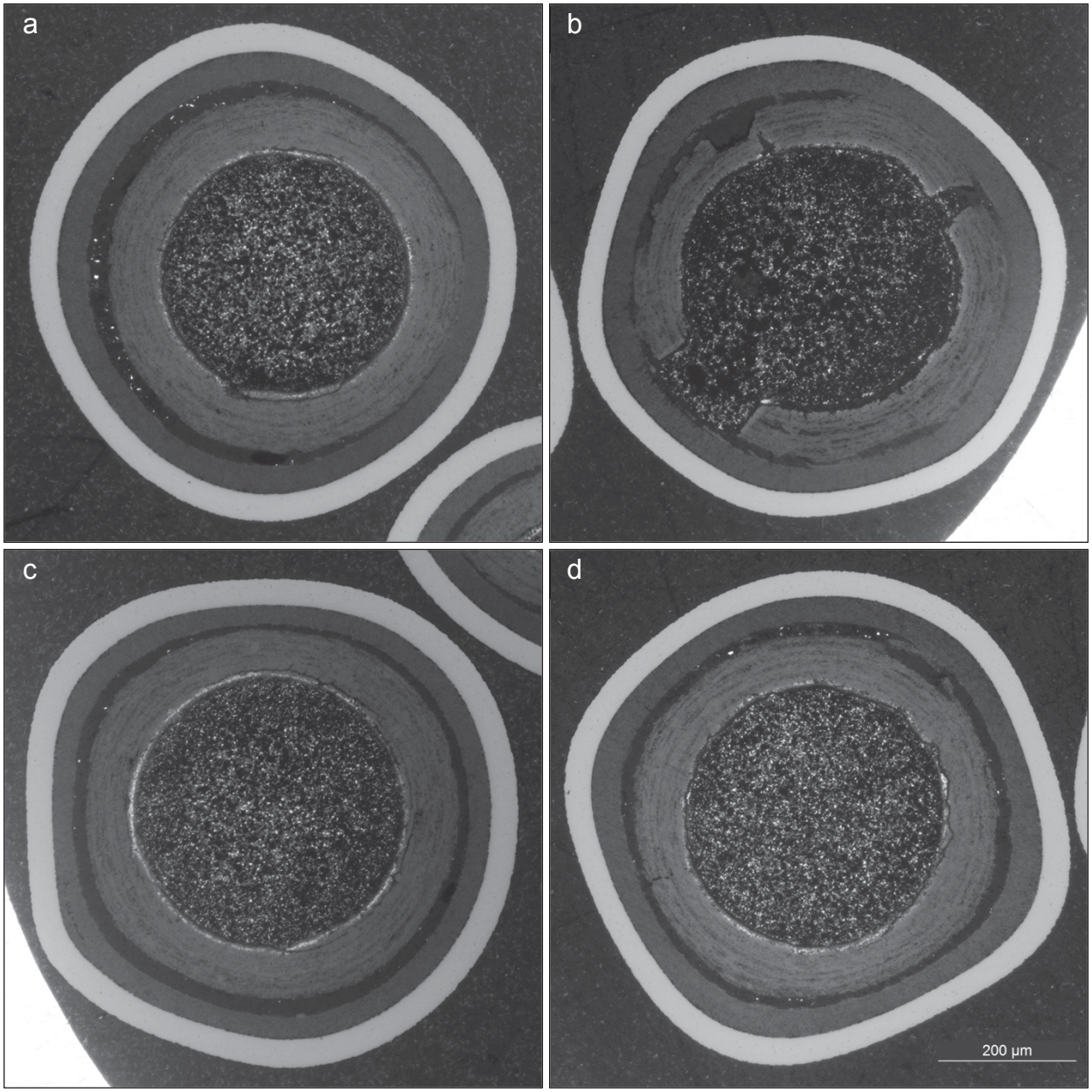

Figure 9. Optical micrographs near midplane of particles from Compact 4-4-3: a) Particle 443-RS30 with very low ^{110m}Ag inventory (M/C = 0.16), b) Particle 443-RS10 with below average ^{110m}Ag inventory (M/C = 0.43), c) Particle 443-RS01 with average ^{110m}Ag inventory that was nevertheless measurably less than calculated (M/C = 0.72), and d) Particle 443-RS15 with high ^{110m}Ag inventory (M/C = 1.24).

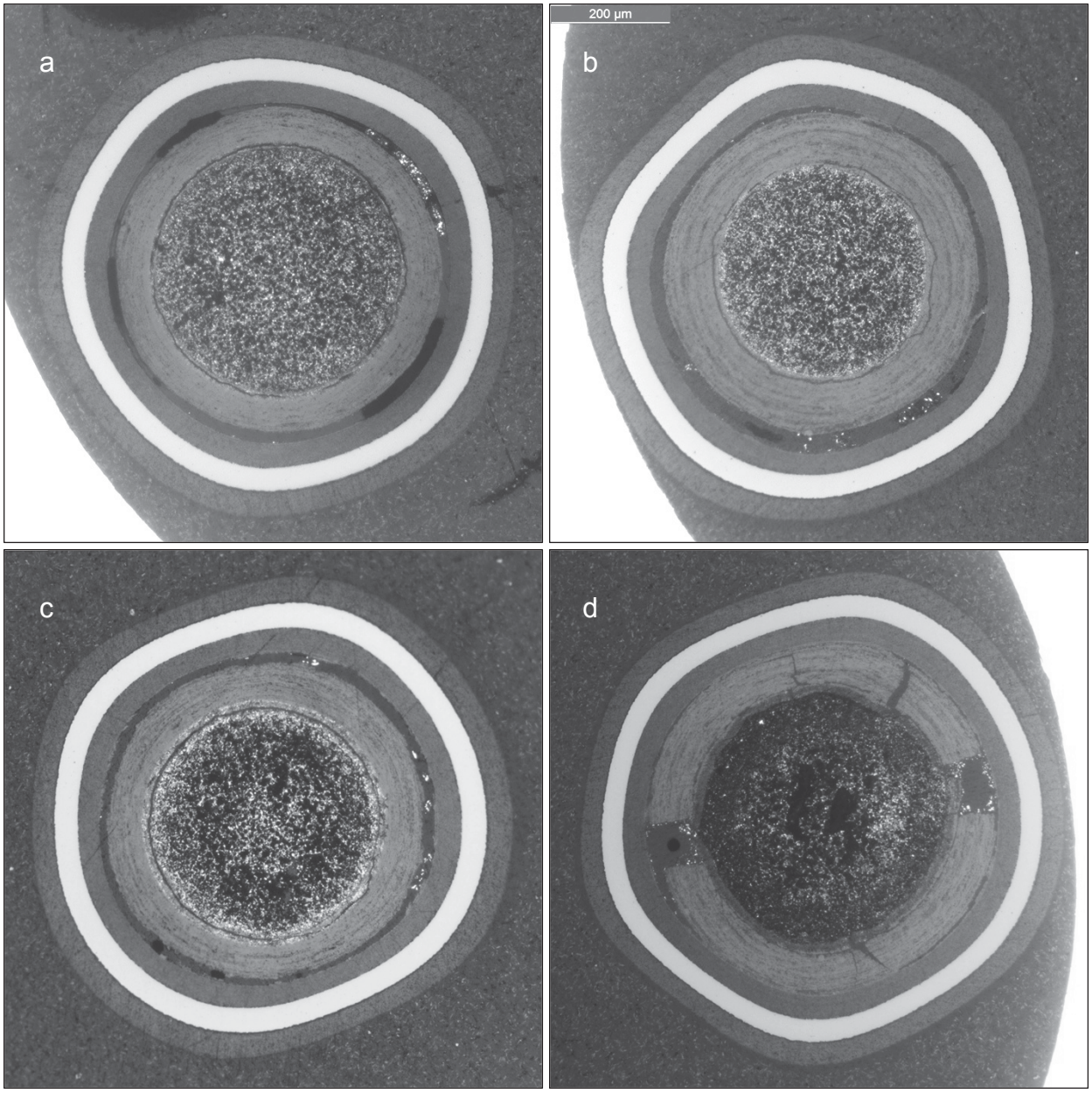

Figure 10. Optical micrographs near midplane of particles from Compact 4-1-2: a) Particle 412-RS40 with very low ^{110m}Ag inventory (M/C = 0.28), b) Particle 412-RS03 with measurably reduced ^{110m}Ag inventory (M/C = 0.56), c) Particle 412-RS07 with measurably reduced ^{110m}Ag inventory (M/C = 0.53), and d) Particle 412-RS44 with high ^{110m}Ag inventory (M/C = 1.12).

SEM on particles from randomly-selected IMGA samples

Figure 11 shows secondary-electron and backscattered electron image pairs centered on a SiC region of the same Compact 4-1-2 particles shown in Figure 10. The interlaced nature of the IPyC/SiC interface is evident in the SEI images, where SiC infiltrated the open porosity at the IPyC surface during deposition; this interface appears undisturbed by the irradiation, as is typical for AGR-1 test fuel. There is a small epoxy-filled gap between the SiC and OPyC layers, which has been attributed to shrinkage in the compact matrix pulling the weakly-bonded OPyC away from the SiC [Hunn et al. 2013-1]. The BEC images are decorated with bright spots in the SiC indicating increased backscattering from near-surface clusters of elements with higher atomic number (Z) than the surrounding material. These clusters could be seen

throughout the SiC in particles that released silver (Figure 11a and b), but tended to be localized to the IPyC/SiC interface in the particle with a retained ^{110m}Ag inventory above the calculated average (Figure 11c) that presumably released very little or no silver. High-Z clusters analyzed by EDS are indicated in Figure 11 by diamonds (Pd) and squares (U), with dashed lines indicating lower relative peak intensity. Palladium was found in every analyzed cluster within the SiC layer. Uranium was often observed collocated with the palladium in the clusters less than 10 µm from the IPyC/SiC interface. Other elements (not shown) were sometimes observed in the clusters located in the interlaced region between the IPyC and SiC, or in spots in the IPyC layer away from the SiC (clusters isolated in the IPyC often contained uranium but rarely contained palladium).

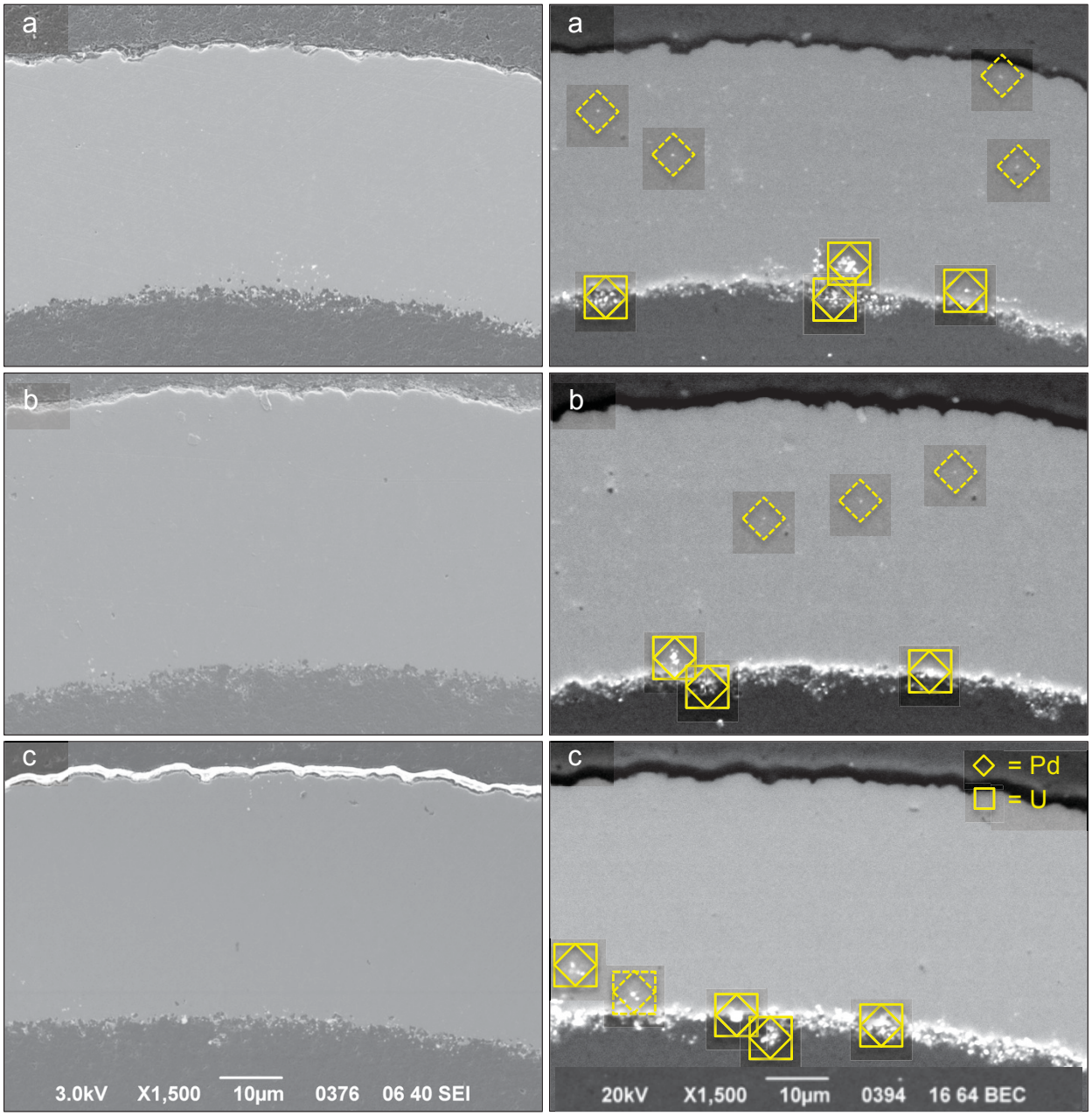

Figure 11. SEI/BEC-paired images near midplane of Compact 4-1-2 particles: a) Particle 412-RS40 with very low ^{110m}Ag inventory (M/C = 0.28), b) Particle 412-RS07 with measurably reduced ^{110m}Ag inventory (M/C = 0.53), and d) Particle 412-RS44 with high ^{110m}Ag inventory (M/C = 1.12). Features circumscribed by a dashed line produced a lower relative EDS intensity from that element.

Figure 12 is a higher resolution optical micrograph of the particle from Compact 4-4-3 with very low ^{110m}Ag inventory shown in Figure 9a; numerous black spots are visible in the SiC. These black spots were observed in all the polished sections of particles selected from Compact 4-4-3. The spots are similar and possibly related to those previously observed in Compact 4-4-1, which was safety tested at a maximum temperature 100°C higher than Compact 4-4-3. In Compact 4-4-1, these spots were identified with SEM analysis to be voids or carbon-filled regions presumably left behind when palladium had moved out of the SiC during the 1800°C Compact 4-4-1 safety test [Hunn et al. 2013-3, page 28].

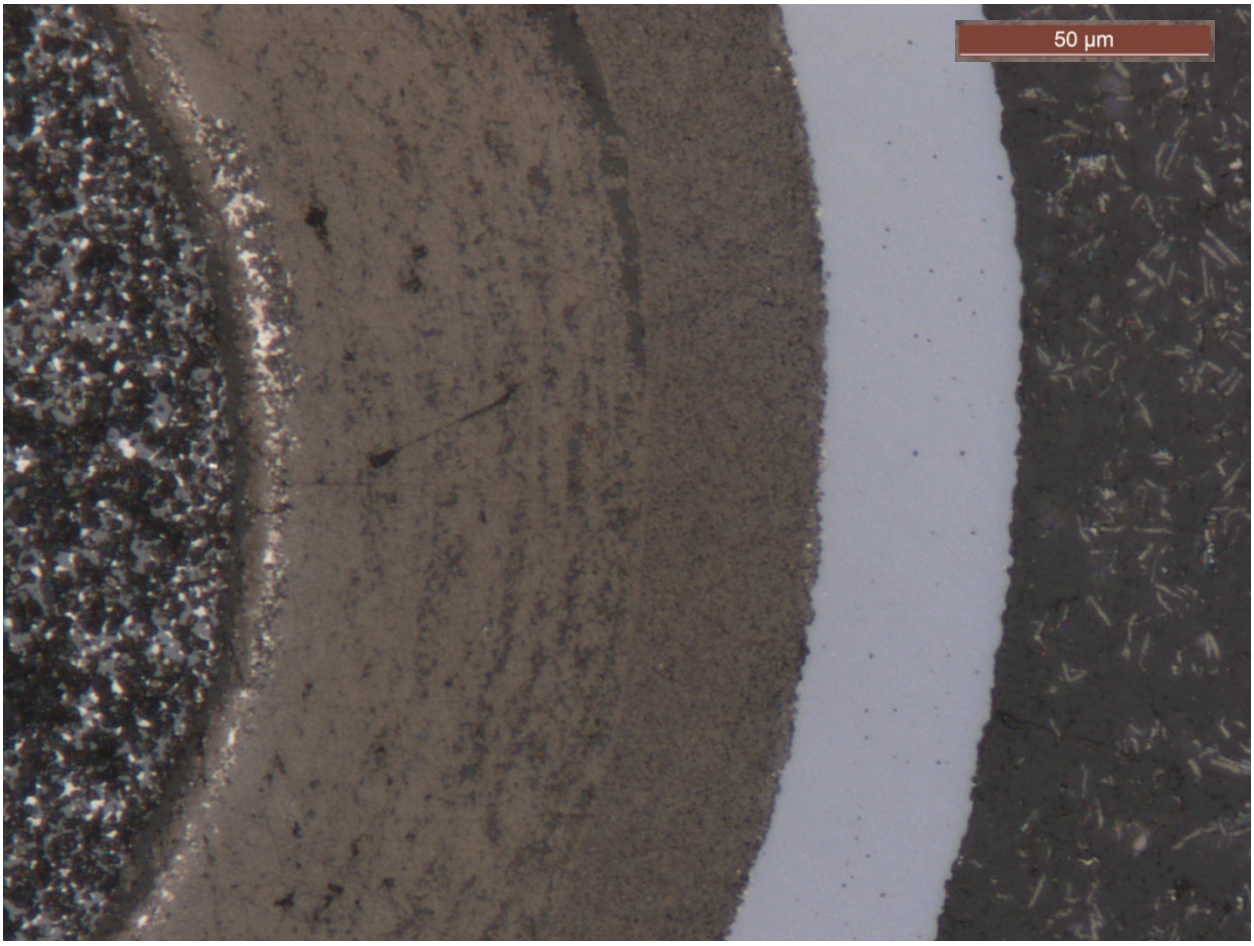

Figure 12. Optical micrograph near midplane of Particle 443-RS30 from Compact 4-4-3 with very low ^{110m}Ag inventory (M/C = 0.16).

Figure 13 shows secondary-electron and backscattered electron image pairs centered on a SiC region of the same Compact 4-4-3 particles shown in Figure 9. Palladium and uranium clusters are identified as in Figure 11, and similar trends were observed: where palladium was readily found throughout the SiC in particles that released measurable ^{110m}Ag, tended to be localized to the IPyC/SiC interface in the particle with better silver retention (note the much lower frequency of faint bright spots in the Figure 13d BEC image, compared to the other particles), and was often collocated with uranium near the IPyC/SiC interface. However, one significant difference between the Compact 4-4-3 and Compact 4-1-2 analyses was that many of the Pd/U clusters near the IPyC/SiC interfaces in particles from Compact 4-4-3 had relatively lower EDS signal from the palladium. In addition, a few clusters in the Compact 4-4-3 particles were observed less than 10 µm from the IPyC/SiC interface, but well within the SiC, that only contained a detectable quantity of uranium. This apparent palladium depletion in the SiC was less dramatic, but still similar to what was observed during analysis of the Compact 4-4-1 particles [Hunn et al. 2013-3], and supports the hypothesis that palladium may be diffusing out during safety testing.

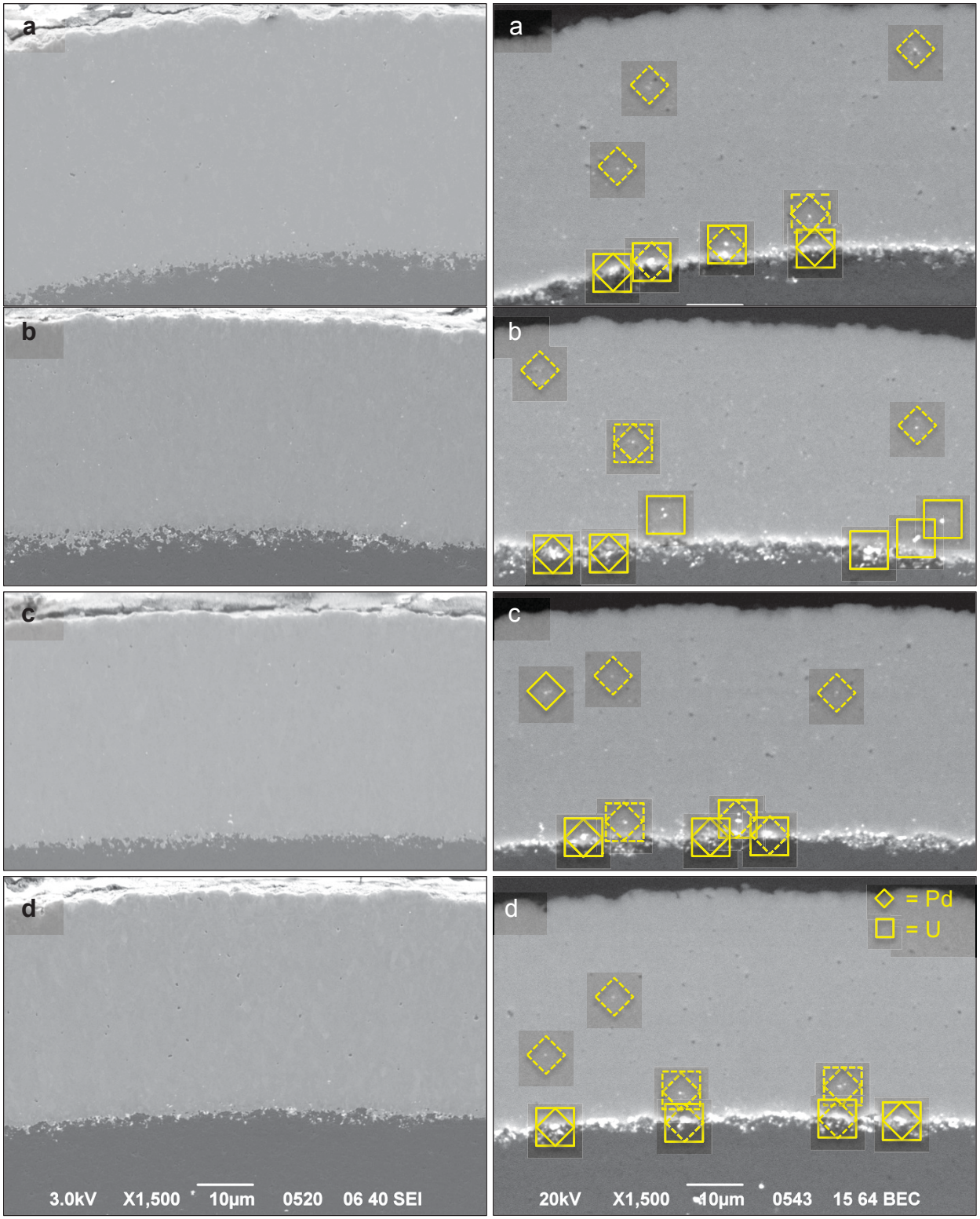

Figure 13. SEI/BEC-paired images near midplane of Compact 4-4-3 particles: a) Particle 443-RS30 with very low ^{110m}Ag inventory (M/C = 0.16), b) Particle 443-RS10 with below average ^{110m}Ag inventory (M/C = 0.43), c) Particle 443-RS01 with average ^{110m}Ag inventory that was nevertheless measurably less than calculated (M/C = 0.72), and d) Particle 443-RS15 with high ^{110m}Ag inventory (M/C = 1.24). Features circumscribed by a dashed line produced a lower relative EDS intensity from that element.

Analysis of particle from Compact 4-1-2 that released cesium during safety test

After IMGA analysis was completed on the particle that released cesium during the Compact 4-1-2 safety test at 1600°C (Particle 412-SP05), it was mounted in epoxy for x-ray tomography. Figure 14 shows a number of planar sections through the particle that reveal a complex internal structure. It is presumed that the missing OPyC came off the particle during the third Soxhlet leach based on negligible ^{85}Kr release during safety testing and indication that the kernel was exposed during this third leaching period. A large fraction of the kernel mass is missing due to the acid infiltration and dissolution. The buffer and IPyC layers did not separate and appear to have fractured as a unit. Delamination of the IPyC from the SiC extends away from the IPyC fracture, eventually leading to fractures in the SiC that start tangential to the IPyC/SiC interface and then tend to curve in a circumferential direction.

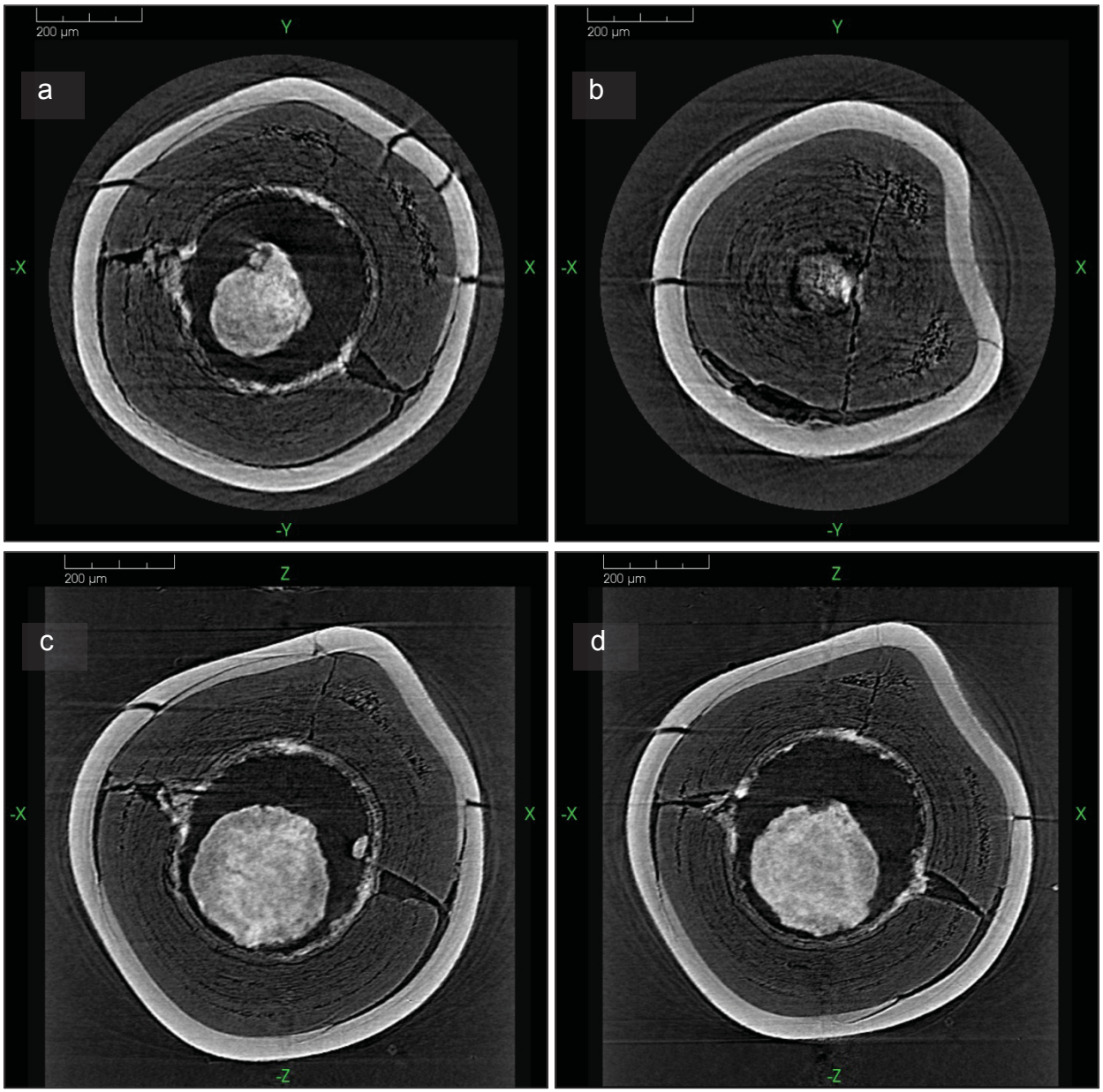

Figure 14. X-ray tomographs through various planes showing the abnormal structure of Particle 412-SP05 from Compact 4-1-2 that released cesium during 1600°C safety testing.

Figure 14 also shows "radial" cracks breaching the SiC layer. Examination of the particle in multiple orientations and slices not shown revealed these cracks to be connected to, and presumably related to, the circumferential cracks in the SiC and the delamination at the IPyC/SiC interface. In the various imaging planes shown in Figure 14, the SiC appears to be breached in numerous locations; however, Figure 15 is a 3D rendering that shows that the SiC through-layer fracture is actually continuous. The breach can be seen radiating out in three directions from location A. The horizontally-oriented crack in the center of the figure circumscribes the particle and runs about halfway around the rim of a dimpled region. At the locations labeled A and B, secondary cracks continue around this dimpled region but do not connect. The dimple was caused by a low-density carbon soot inclusion at the buffer/IPyC interface (Figure 16). Inclusions like this are usually caused by over-fluidized particles contacting the soot-coated walls above the fluidized bed during coating.

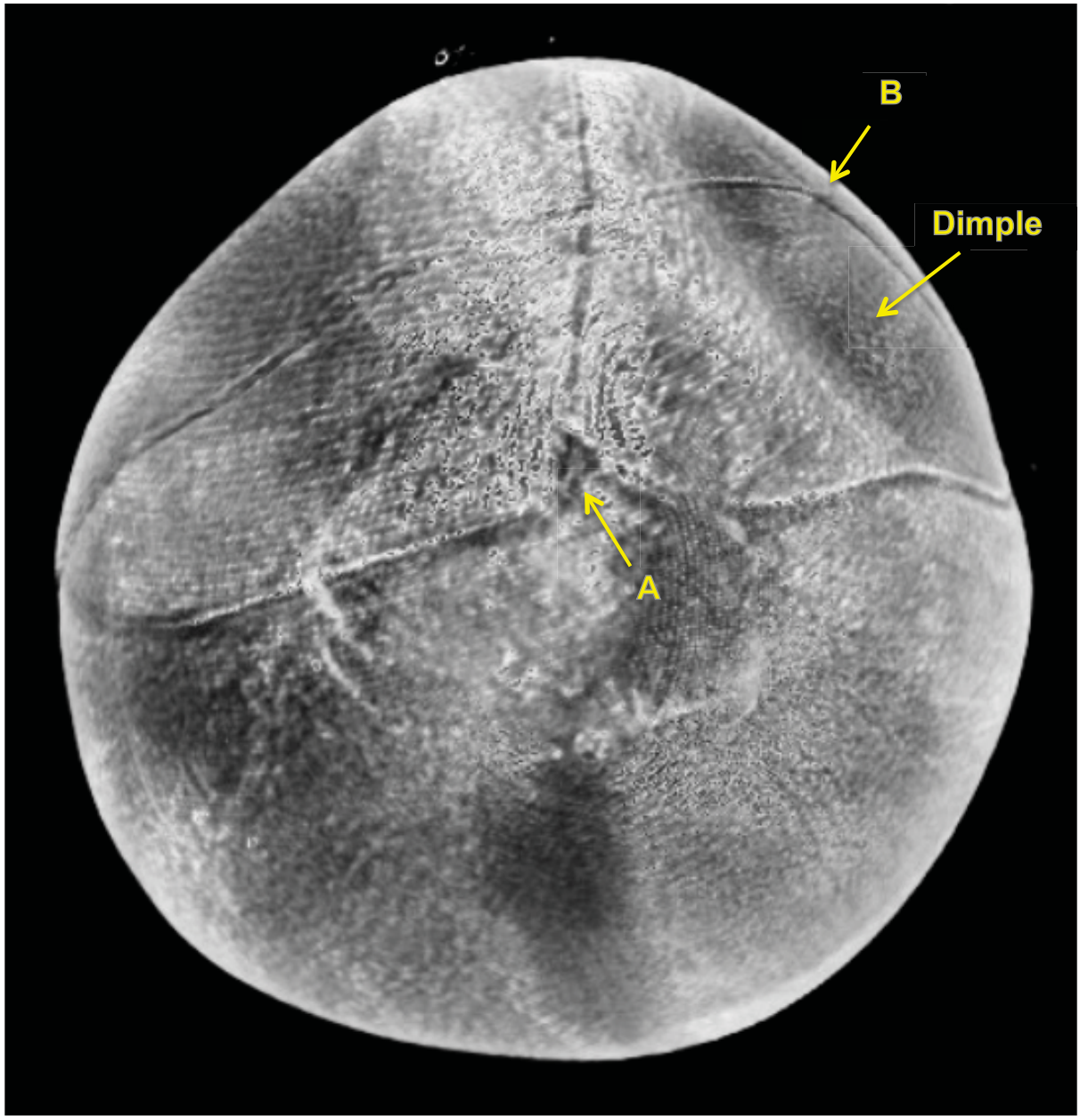

Figure 15. Semitransparent 3D rendering of Particle 412-SP05 showing continuous SiC breach, a portion of which runs along the rim of a dimpled region.

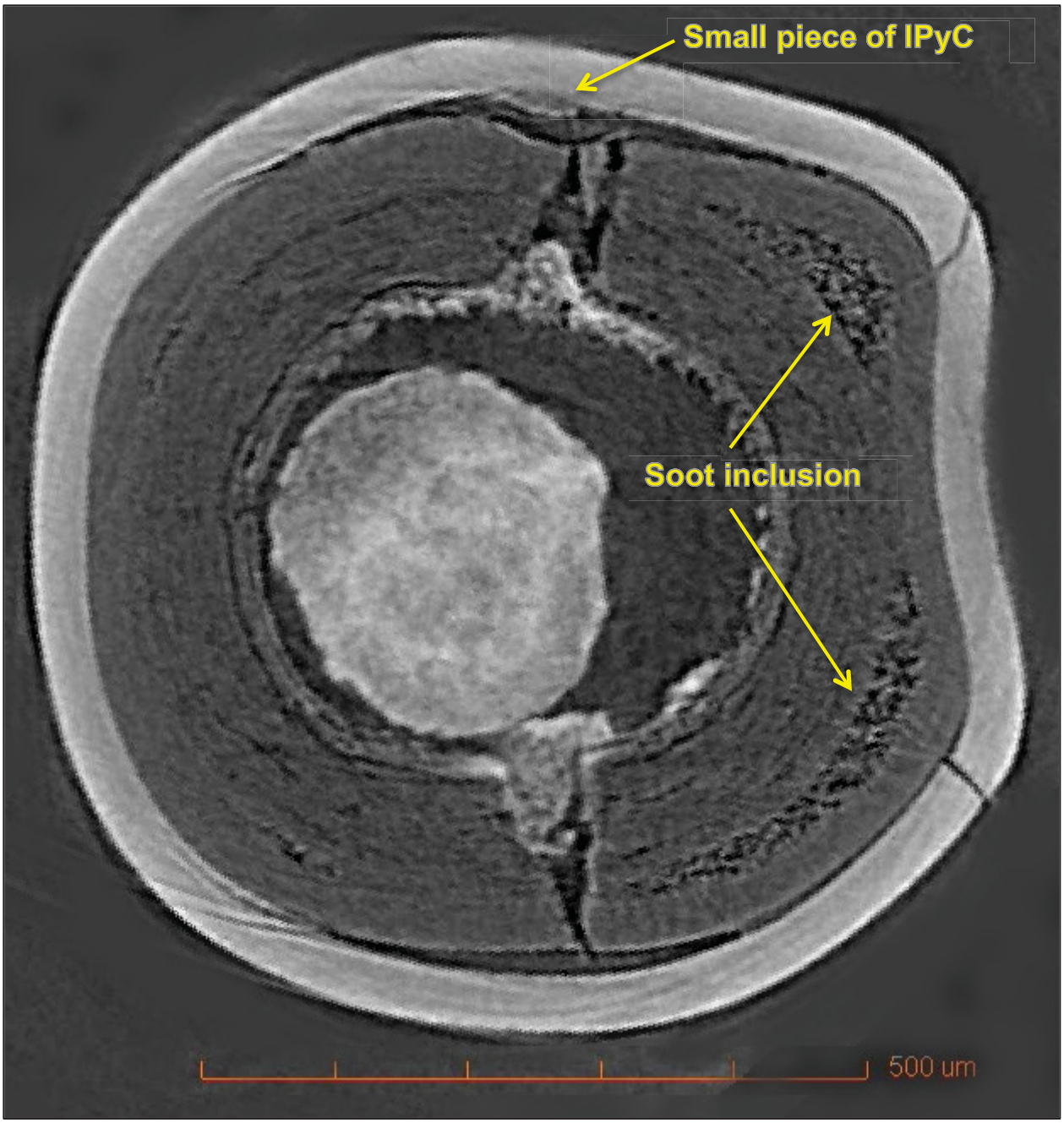

Figure 16. Oblique tomograph through midplane of Particle 412-SP05 showing the carbon soot inclusion that was responsible for abnormal particle shape.

Figure 16 shows that the IPyC/SiC delamination terminates near the rim of the dimple, close to where the SiC breach intersects the interface. Also of interest in this figure are the small section of IPyC that did not pull away from the SiC at the tip of the upper buffer/IPyC fracture and the residual portions of kernel protruding into the buffer/IPyC fractures that were not removed during acid dissolution of a large fraction of the kernel. The fact that portions of the kernel remained here and around the entire inside surface of the buffer suggests that this residual material was less soluble in hot nitric acid then other parts of the kernel. To further investigate the internal microstructure of Particle 412-SP05 and analyze the residual kernel chemistry, the particle was mounted and sectioned for SEM using the 3D x-ray imaging as a guide to orient the particle and grind down to an area of interest.

Figure 17 shows an optical image of a section near the midplane from Particle 412-SP05 after diamond grinding/polishing and an SEM-BEC image after an additional 5-minute polish with colloidal silica. A portion of SiC is missing at the lower left corner of the images because it was a piece that was completely separated due to the continuous fracture in the SiC and it did not extend far enough below the polish plane to be retained by the epoxy during polishing. Low-density carbon soot inclusions can be seen in various locations between the buffer and IPyC.

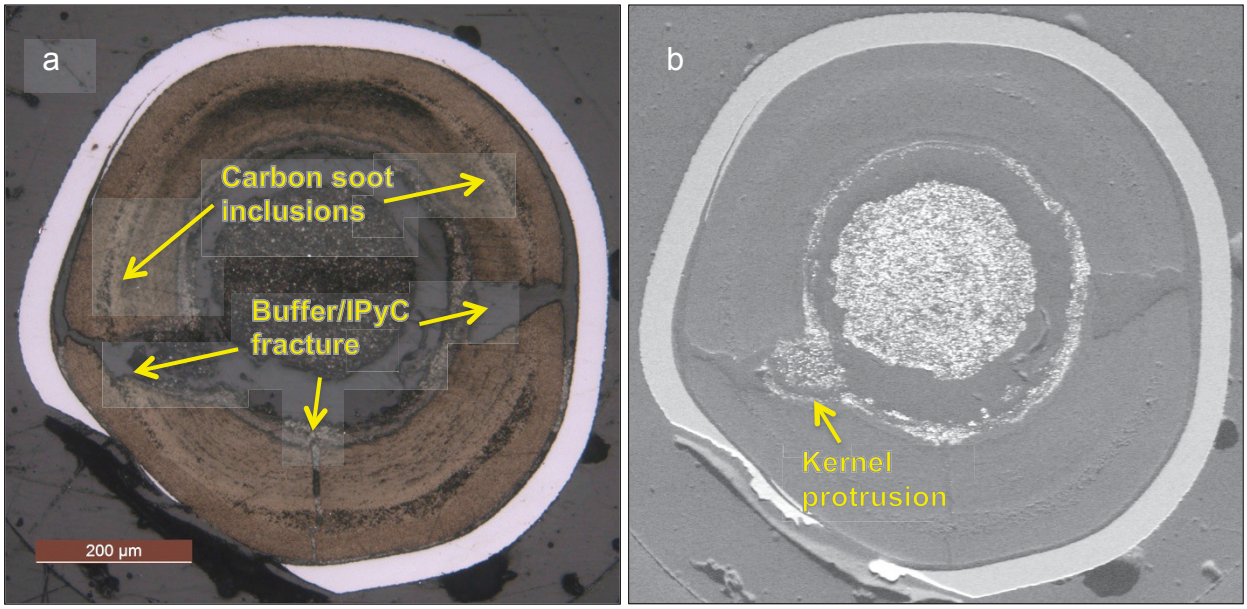

Figure 17. Optical/SEM-BEC image pair of polished section from Particle 412-SP05.

Three intersections with buffer/IPyC fractures can be seen in Figure 17. These features are mostly filled with the vacuum backpotting epoxy. Two are arrowhead-shaped fractures that lead to regions of IPyC/SiC delamination; x-ray inspection shows that these two features are actually intersections through one continuous fracture that separates the buffer/IPyC roughly in two. In this polish plane, kernel protrusion into the gap between the buffer/IPyC halves can be seen in one of the features. The third feature (bottom of image) intersects a buffer fracture that lies in a plane roughly perpendicular to the larger fracture and 3D inspection by x-ray revealed that it is only present in one of the buffer/IPyC halves. This narrow fracture is visible as a black line in the x-ray tomographs in Figure 14.

The SEI/BEC image pairs in Figure 18 show the large buffer/IPyC fracture and a region of IPyC that was pulled away from the IPyC/SiC interface (left side of images in Figure 17). In Figure 18, a small region of IPyC that is still bonded to the SiC can be seen at the tip of the buffer/IPyC fracture. It is apparent that the IPyC/SiC separation progressed away from the tip of the buffer/IPyC fracture and eventually led to a tangential crack in the SiC which continued to propagate circumferentially through the SiC. Figure 19 shows where the IPyC initially started separating from the SiC, leaving portions of IPyC still attached to the SiC (left), and where the IPyC/SiC delamination crossed into the SiC layer (right).

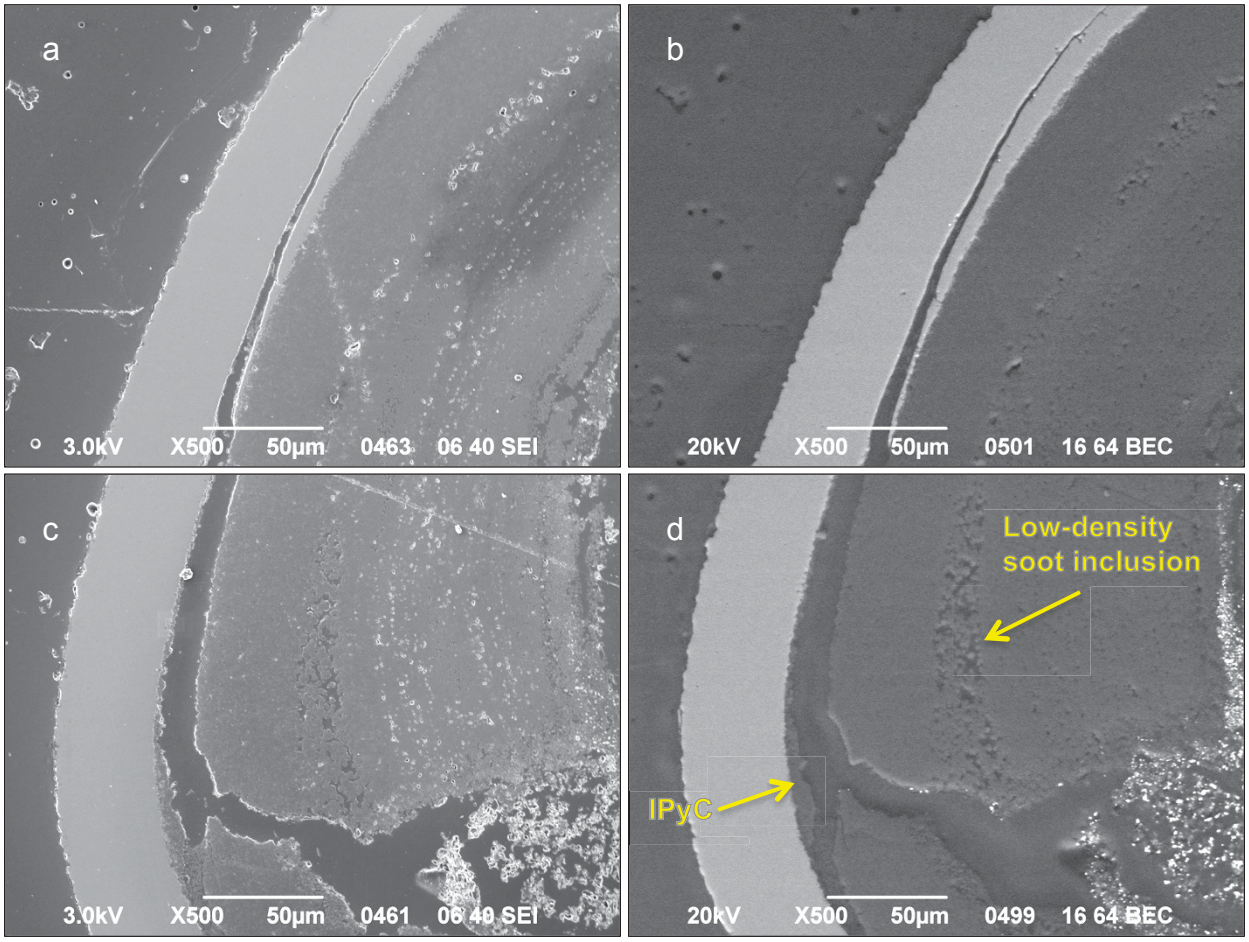

Figure 18. SEI/BEC-paired images near midplane of Particle 412-SP05.

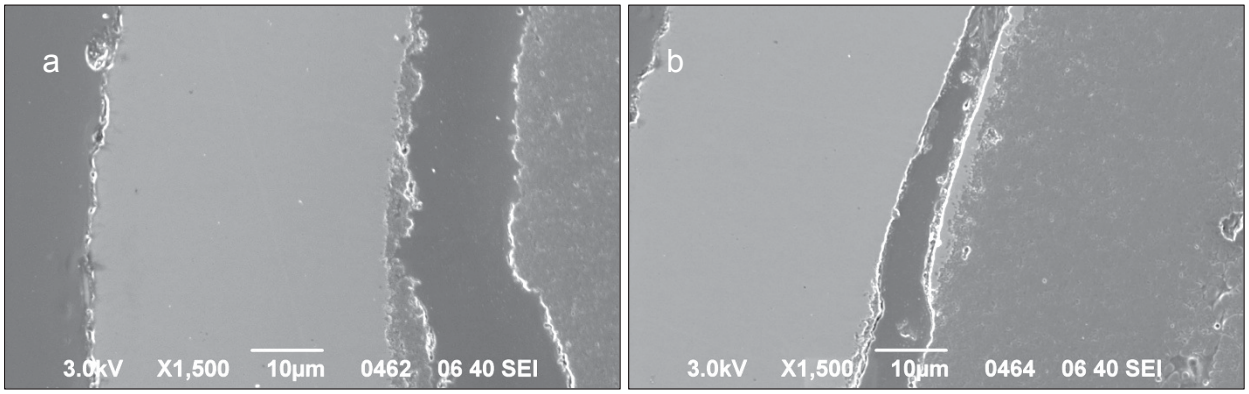

Figure 19. SEI images of Particle 412-SP05 showing magnified regions of Figure 18.

Few high-Z clusters were observed in the layers of Particle 412-SP05, which is very unusual compared to what was observed in the randomly-selected Compact 4-1-2 particles and almost every particle examined from other AGR-1 compacts. Figure 20 shows an undamaged region of the IPyC/SiC interface. The BEC image is relatively void of bright spots from high-Z clusters compared to those seen in Figure 11. Bright spots in the SEI image that do not appear as bright spots in the BEC image are artifacts from small pieces of debris on the surface of the polished sample. Figure 21 is an SEI/BEC image pair showing the tip of the SiC fracture that was imaged at lower resolution in Figure 18. Again, relatively few high-Z clusters are evident at the IPyC/SiC interface, but a few bright spots can be seen decorating what looks like small corrosion regions along the SiC crack. These bright spots were determined by EDS to be predominantly uranium (Si, C, and O peaks were also present in the analyzed volumes). The reason for the absence of palladium that one would assume to have been present in these regions is unknown.

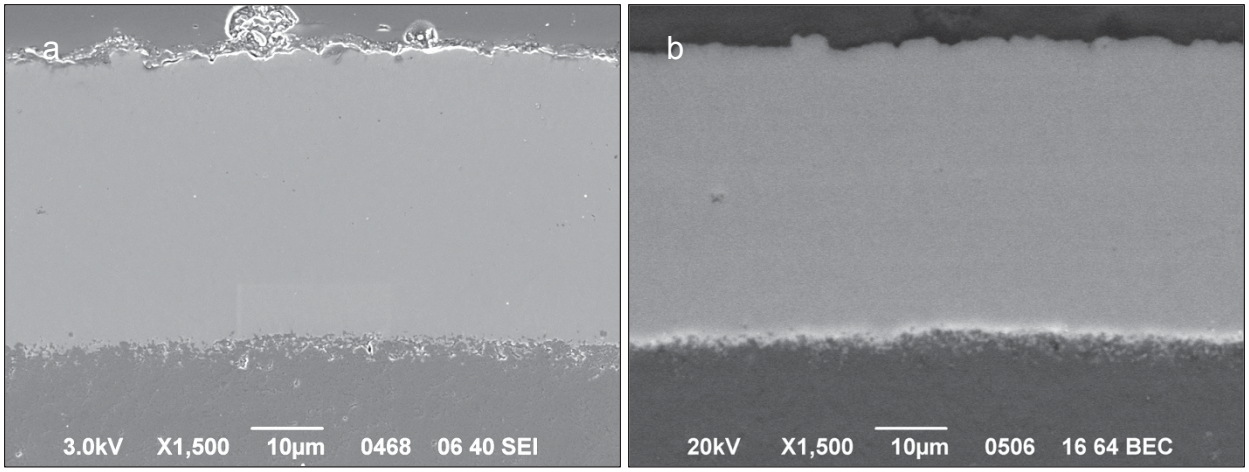

Figure 20. SEI/BEC-paired images near midplane of Particle 412-SP05.

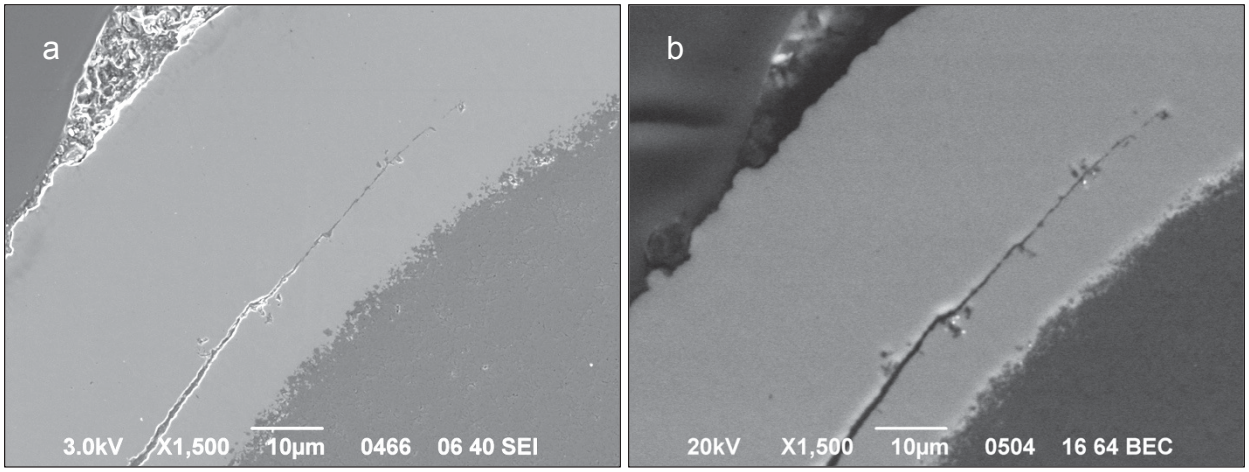

Figure 21. SEI/BEC-paired images near midplane of Particle 412-SP05.

Residual kernel material in the center of the Particle 412-SP05 kernel, at the inside surface of the buffer, and in the protruded region (Figure 17) was analyzed by EDS; spectra obtained from these three locations were nearly identical (Figure 22a). However, comparison to EDS spectra in Figure 22b shows that the relative abundance of several elements (especially uranium) remaining in the Particle 412-SP05 kernel was significant different from kernels in randomly-selected particles. Figure 23 shows the most abundant elements (after uranium) expected to have been produced by the AGR-1 irradiation of the Compact 4-1-2 fuel kernels, plotted as a fraction of the calculated uranium content at the end of irradiation. Uranium

dominated the EDS spectra obtained from kernel material in the randomly-selected particles (Figure 22b), and only the three highest abundance metallic species from Figure 23 (Zr, Mo, and Nd) were detected above the uranium signal. Peaks from silicon and aluminum are most likely due to foreign material trapped in the kernel pores, probably residual silica from the final polish and grinding debris from the SiC layer and aluminum holder. Carbon and oxygen peaks may also include contributions from these and other sources external to the kernel, with carbon being particular susceptible to contribution from the backpotting epoxy. In contrast to the typical kernels, the relative uranium signal in the Particle 412-SP05 kernel spectra (Figure 22a) was drastically reduced, presumably due to removal of more than 90% of a single kernel's inventory of uranium through acid leaching during the third Soxhlet extraction (Table 3). More than 50% of a single kernel's inventory of ^{95}Zr and ^{146}Nd were also detected in the third Soxhlet leachate, and the primary EDS peaks from these elements are also absent in Figure 22a. The lower background from uranium allowed resolution of a series of peaks from ruthenium, palladium, and possibly rhodium. Significant quantities of these elements were not detected during the third leach, and IMGA measurements determined that ^{106}Ru was mostly retained in Particle 412-SP05 (Table 4).

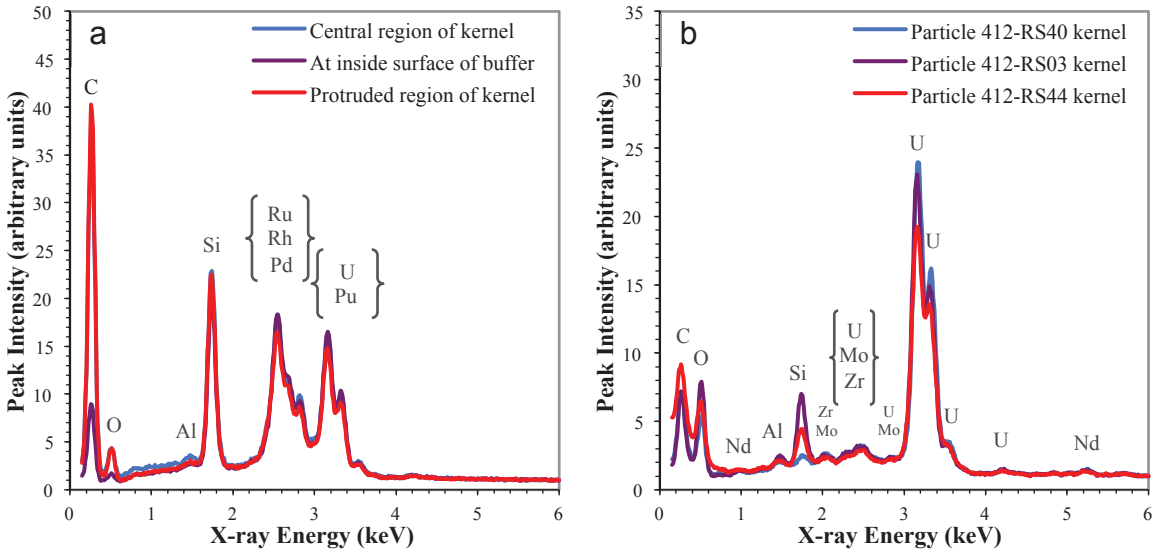

Figure 22. EDS spectra of Compact 4-1-2 kernel material; a) Particle 412-SP05 that lost cesium during safety testing and whose kernel was acid leached, and b) particles with unleached kernels. Elements that may have significantly contributed to each peak are identified.

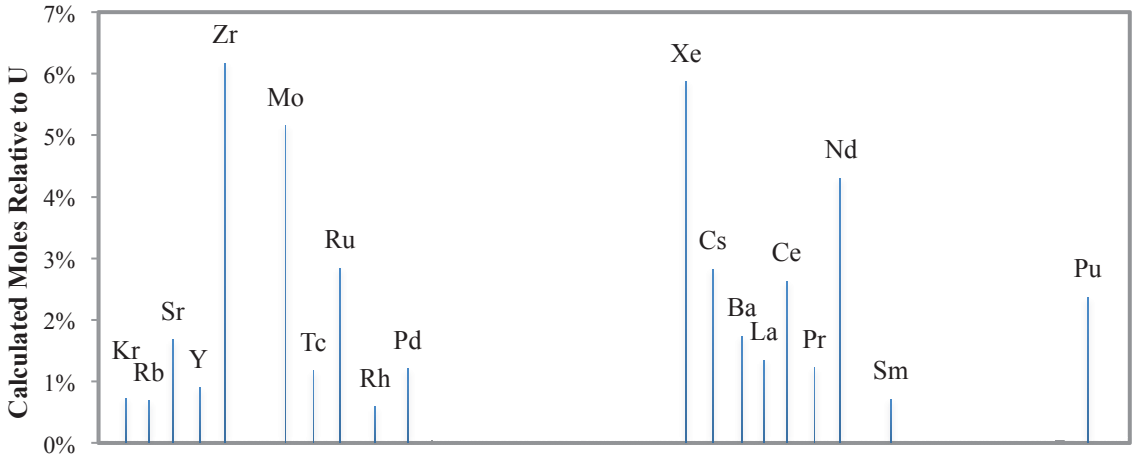

Figure 23. Average calculated molar fraction of elements in Compact 4-1-2 two years after irradiation [Sterbentz 2013], plotted relative to uranium (only elements >0.5% shown).

Summary and Conclusions

Safety testing and post-safety testing PIE on two more compacts from the AGR-1 irradiation test have been completed and results are summarized in this report; additional results and discussion will appear in individual PIE reports for each compact and in a final AGR-1 PIE summary report. Safety tests were performed at 1600 and 1700°C on Compacts 4-1-2 and 4-4-3, respectively. Post-safety testing PIE consisted of DLBL, IMGA, x-ray tomography, and materialographic inspection by mechanical cross sectioning followed by optical and electron microscopy. Data was obtained on radioisotope retention and microstructural changes that occurred during irradiation and the subsequent safety testing.

None of the safety tests resulted in significant ^{85}Kr release, indicating that at least one of the three gas-tight outer layers of the TRISO coating on each particle (IPyC, SiC, or OPyC) remained intact throughout the duration of each test. No significant cesium release was observed during the 1700°C safety test of Compact 4-4-3 (Figure 3), indicating that all particles had intact SiC layers. In the 1600°C test of Compact 4-1-2, cesium release was detected that appeared to be from 1–2 particles with a breached SiC (Figure 2). Post-safety testing PIE determined that the cesium release came from one particle with an as-fabricated defect that experienced through-wall SiC fracture after the compact was heated to 1600°C.

Significant quantities of silver and europium were released from the compacts during both safety tests, far beyond what can be attributed to breaches through the SiC layer (Table 1). Strontium release was also detected during both tests, more in the 1700°C test. During the 1600°C safety test of Compact 4-1-2, silver appeared to come out of the compact immediately upon heating, but then no further significant release occurred; during the 1700°C safety test of Compact 4-4-3, a second release of silver was observed after the temperature was cycled from 1700–20–1700°C (Table 2). Collection of europium and strontium on the deposition cups occurred over a longer time period. The ^{110m}Ag detected at the beginning of the 1600°C and 1700°C tests, and the europium and strontium collected on the deposition cups throughout these tests, were probably coming from the compact matrix, as opposed to transport through intact SiC layers. Silver and europium are known to escape through intact SiC during irradiation, and the quantities detected during the safety tests were in the range of what has been detected by LBL in the matrix of as-irradiated compacts not subjected to safety testing [Hunn et al. 2012-1; Hunn et al. 2013-1]. The secondary release of silver related to the thermal cycling has been observed in other tests [Hunn et al. 2012-2], and may have been due to silver release through intact SiC.

The defective particle in Compact 4-1-2 was recovered for microstructural analysis by electrolytically deconsolidating the compact matrix and surveying 4079 particles with IMGA (Figure 4). This particle was recovered mostly intact, but the OPyC layer was missing and had apparently fractured during a third Soxhlet extraction prior to IMGA, which resulted in partial leaching of the kernel. During this third extraction, more than 90% of the uranium was leached from the kernel by the nitric acid; other isotopes leached from the kernel included significant fractions (>50%) of the expected single particle inventories for ^{95}Zr, ^{140}Ce, ^{144}Ce, ^{141}Pr, ^{146}Nd, ^{152}Sm, ^{239}Pu, ^{240}Pu, and small fractions (<10%) of the expected single particle inventories for ^{90}Sr, ^{106}Ru, ^{125}Sb, ^{134}Cs, ^{137}Cs, ^{154}Eu (Table 3). IMGA showed that some ^{106}Ru and ^{125}Sb activity remained in the defective particle in agreement with the lower leached fractions of these elements, but measured activities for ^{110m}Ag, ^{134}Cs, ^{137}Cs, and ^{154}Eu were very low due to release during safety testing and ^{144}Ce activity was very low due to acid leaching, possibly combined with some release during safety testing (Table 4). X-ray analysis of the defective particle showed that a significant volume of material had been removed from the kernel (Figure 14); and EDS analysis of the residual kernel material detected measurable depletion of uranium, zirconium, and neodymium in agreement with the removal of these elements detected by acid leaching, while ruthenium remained in agreement with the acid leaching and IMGA results (Figure 22).

Although the progression of the microstructural development in the Compact 4-1-2 defective particle could not be directly observed, some presumptions can be made based on the observed microstructure in this and other AGR-1 particles. It is likely that fracture of the buffer and IPyC layers, followed by the

IPyC/SiC delamination and tangential/circumferential fracture in the SiC, occurred during irradiation. All these features have been observed in as-irradiated particles [Ploger et al. 2012; Hunn, Savage, and Kehn 2012]. Through-layer (radial) fracture of the SiC would not have been present during irradiation (based on the lack of significant cesium release in Capsule 4). Cesium release during safety testing (Figure 2) indicated that the SiC in the defective particle was probably breached soon after reaching 1600°C. The observed radial fracture through the SiC appeared to be related to the abnormal coating shape caused by the soot inclusion at the buffer/IPyC interface. The as-irradiated structure prior to radial SiC fracture during safety testing may have also been partially related to the dimpled coating; some of the boundaries of the delamination between the IPyC and SiC terminated along the rim of the dimple, which may have increased the likelihood for SiC fracture at this location. Based on the good ^{85}Kr retention during safety testing and initial low concentration of exposed uranium in the first two acid leachates (Table 3), fracture of the OPyC layer must have occurred during the third Soxhlet extraction; removal of the fractured OPyC layer could have occurred at this time or during subsequent handling to separate particles from the matrix residue prior to IMGA.

Microstructures observed in randomly-selected particles extracted from both of the safety tested compacts were similar to those seen in as-irradiated fuel [Ploger et al. 2012; Hunn, Savage, and Kehn 2012; Hunn et al. 2013-1]. Shrinkage of the buffer layer and swelling of the kernel were common to all particles, with the associated varied degrees of buffer/IPyC delamination and periodic cases of buffer fracture, which was usually accompanied by portions of the kernel protruding into a gap between the buffer fragments. None of these microstructures seemed to be directly related to the varied amount of silver released from the particles selected for examination. SEM imaging and EDS analysis of the SiC layers showed palladium and uranium trapped in the SiC layer. Particles with lower ^{110m}Ag inventories had numerous clusters of palladium scattered throughout the layer, while particles with ^{110m}Ag inventories higher than the calculated average (indicating low silver release) had SiC layers relatively void of palladium clusters more than 10 μm away from the IPyC/SiC interface (Figure 11 and Figure 13). Uranium tended to be constrained to clusters close to the IPyC/SiC interface, and uranium in the SiC was typically collocated with palladium. Particles from Compact 4-4-3 had clusters with significantly more uranium than palladium, which may indicate that palladium is exiting the SiC during 1700°C safety testing. This apparent out-diffusion of palladium was particularly evident in particles from the first 1800°C safety test on Compact 4-4-1 [Hunn et al. 2013-3].

Acknowledgment

This work was supported by the U.S. Department of Energy, Office of Nuclear Energy, under the Very High Temperature Reactor Technology Development Office Advanced Gas Reactor Fuel Development and Qualification Program. Analysis of leach solutions and CCCTF furnace components was provided by the ORNL Nuclear Analytical Chemistry & Isotopics Laboratory. Hot cell activities were supported by the staff of the ORNL Irradiated Fuels Examination Laboratory.

References

Baldwin, C.A., et al. 2012. “First Elevated Temperature Performance Testing of Coated Particle Fuel Compacts from the AGR-1 Irradiation Experiment.” HTR2012-3-027. *Proceedings of the HTR 2012.* Tokyo, Japan October 28–November 1, 2012.

Collin, B.P. 2012, *AGR-1 Irradiation Test Final As-Run Report.* INL/EXT-10-18097, Rev. 1. Idaho National Laboratory, Idaho Falls, ID.

Harp, J.M. 2013. *Analysis of Individual Compact Fission Product Inventory and Burnup of the AGR-1 TRISO Experiment Using Gamma Spectrometry*. INL/ECAR-1682, Rev. 2. Idaho National Laboratory, Idaho Falls, ID.

Hawkes, G.L. 2012. *AGR-1 Daily As-Run Thermal Analyses*. INL/ECAR-968, Rev. 3. Idaho National Laboratory, Idaho Falls, ID.

Hunn, J.D., T.W. Savage, and J.S. Kehn 2012. *AGR-1 Irradiated Compact 6-4-2 PIE Report: Preparation and Analysis of Polished Compact Sections*. ORNL/TM-2012/285, Rev. 0. Oak Ridge National Laboratory, Oak Ridge, TN.

Hunn, J.D. et al. 2012-1. *AGR-1 Irradiated Compact 6-1-1 PIE Report: Evaluation of As-Irradiated Fuel Performance using Leach Burn Leach, IMGA, Materialography, and X-ray Tomography*. ORNL/TM-2012/233. Oak Ridge National Laboratory, Oak Ridge, TN.

Hunn, J.D. et al. 2012-2. *Safety Tests on Irradiated AGR-1 Compacts 3-3-2, 3-2-2, and 6-2-1*. ORNL/LTR-2012/396. Oak Ridge National Laboratory, Oak Ridge, TN.

Hunn, J.D. et al. 2012-3. *PIE on Five Irradiated AGR-1 Compacts*. ORNL/LTR-2012/397. Oak Ridge National Laboratory, Oak Ridge, TN.

Hunn, J.D. et al. 2013-1. *AGR-1 Irradiated Compact 4-4-2 PIE Report: Evaluation of As-Irradiated Fuel Performance with Leach Burn Leach, IMGA, Materialography, and X-ray Tomography*. ORNL/TM-2013/236. Oak Ridge National Laboratory, Oak Ridge, TN.

Hunn, J.D. et al. 2013-2. *Safety Tests on Irradiated AGR-1 Compacts 4-1-2, 4-4-3, and 4-4-1*. ORNL/LTR-2013/290. Oak Ridge National Laboratory, Oak Ridge, TN.

Hunn, J.D. et al. 2013-3. *PIE on Three Irradiated AGR-1 Compacts in FY2013*. ORNL/LTR-2013/291. Oak Ridge National Laboratory, Oak Ridge, TN.

Ploger, S.A. et al. 2012. *Ceramographic Examinations of Irradiated AGR-1 Fuel Compacts*. INL/EXT-12-25301, Rev. 1. Idaho National Laboratory, Idaho Falls, ID.

Sterbentz, J.W. 2013. *JMOCUP As-Run Daily Depletion Calculation for the AGR-1 Experiment in ATR B-10 Position*. INL/ECAR-958, Rev. 2. Idaho National Laboratory, Idaho Falls, ID.